Causal geodesics in cylindrically symmetric vacuum spacetimes using Hamilton-Jacobi formalism

Ashiqul Islam Dip,[1,2,*] Nishat Anjum,[3,4,†] Maruf Ahmed,[1,4,‡] and Iffat Zumarradah[5,4,§]

[1]*Division of Research, Community of Physics, Kallyanpur, Dhaka 1207, Bangladesh*
[2]*Department of Physics, North Carolina State University, Raleigh, North Carolina 27607, USA*
[3]*Division of Academics, Community of Physics, Kallyanpur, Dhaka 1207, Bangladesh*
[4]*Department of Physics, University of Dhaka, Dhaka 1000, Bangladesh*
[5]*Division of Administration, Community of Physics, Kallyanpur, Dhaka 1207, Bangladesh*

(Received 31 December 2021; revised 21 January 2024; accepted 1 August 2024; published 11 September 2024)

Cylindrically symmetric vacuum spacetimes are of immense interest in theoretical physics due to their connection to cosmic strings hypothesized in quantum field theory. In this article, we explore the properties of such a spacetime and provide the complete, exact solution by quadrature to the timelike and lightlike geodesics in it, using the Hamilton-Jacobi formalism. In addition, we compare several properties of massive particle trajectories in relativistic cylindrically symmetric vacuum spacetimes to their nonrelativistic, Newtonian gravitational counterparts. On top of that, we devise a classification scheme and use it to categorize the orbits of massive particles.

DOI: 10.1103/PhysRevD.110.064040

I. INTRODUCTION

Since their first realization by Kibble [1] in 1976, cosmic strings have intrigued many cosmologists and relativists. Cosmic strings are one-dimensional topological defects, formed in the early Universe due to a symmetry breaking phase transition [1–4]. These primordial cosmic line defects potentially form a string network at a cosmological scale [5,6]. Their vibrations might produce gravitational waves, radiating a stochastic gravitational-wave signature across the Universe [3,7–9]. Even though it is likely that cosmic strings exist, the probability of finding one is very small [10,11]. However, in recent years, the hope of detecting cosmic strings by means of gravitational waves has risen due to the direct detection of gravitational waves by the LIGO and Virgo collaborations [12–14]. Furthermore, the recently released 12.5-year data set of the NANOGrav Collaboration might suggest the very first detection of cosmic strings and hence their existence, according to some authors [15–17].

An infinitely long, straight (idealized) cosmic string gives rise to a cylindrically symmetric spacetime around it [18–20]. However, the discovery of a cylindrically symmetric vacuum solution to Einstein's equation dates back to 1919 and is called the Levi-Civita spacetime, named after its discoverer [21,22]. In 1958, Marder proved that the Levi-Civita solution possesses two independent parameters [22,23]. Considering the mostly positive sign convention, the metric tensor in the Levi-Civita spacetime can be written as [24–26]

$$\mathbf{ds}^2 = -\xi^{4\sigma}\mathbf{d}t \otimes \mathbf{d}t + (1-2\sigma)^2 P^2 \xi^{8\sigma^2-4\sigma}\mathbf{d}\xi \otimes \mathbf{d}\xi + P^2\xi^{2-4\sigma}\mathbf{d}\phi \otimes \mathbf{d}\phi + \xi^{8\sigma^2-4\sigma}\mathbf{d}z \otimes \mathbf{d}z, \tag{1}$$

where $-\infty < t < \infty$, $0 \le \xi < \infty$, $0 \le \phi \le 2\pi$, and $-\infty < z < \infty$, with $\phi = 2\pi$ identified as $\phi = 0$. The above-mentioned metric tensor contains two independent parameters, σ and P, where σ is dimensionless and P has the dimension of length. For an infinitely long linear mass distribution [27], the parameter $\sigma \in [0, 1/2]$ determines the linear mass density μ via the relation [28]

$$\mu = \frac{\sigma}{1-2\sigma+4\sigma^2} \tag{2}$$

and is known as the mass parameter. On the other hand, the parameter $P \in [1, \infty)$ carries the information about the "deficit angle" of the Levi-Civita spacetime [25]. For $\sigma = 0$ and $P = 1$, the Levi-Civita spacetime reduces to the Minkowski spacetime; for $\sigma = 0$ but $P \neq 1$, it represents the spacetime around an idealized cosmic string, as one easily sees.

There have been multiple attempts to find the geodetic motion in other cylindrically symmetric spacetimes. In the late 1990s, Herrera and Santos derived a circular geodetic motion of massive particles in Lewis spacetime [29]. In 2014, Brito *et al.* found the solution to the geodesic

*Contact author: dip@cpbd.ac
†Contact author: nishat@cpbd.ac
‡Contact author: maruf@cpbd.ac
§Contact author: iffat@cpbd.ac

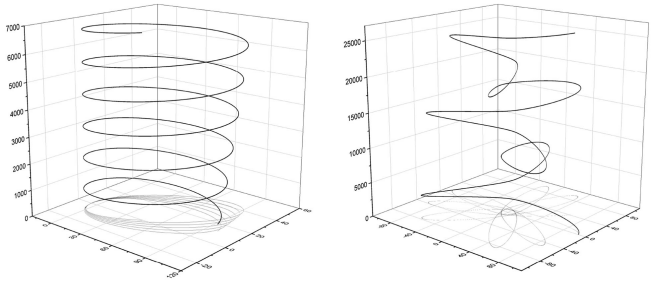

(a) (b)

FIG. 1. Trajectories of particles moving in Levi-Civita spacetime. The thick black curves are the original trajectories, while the thin gray curves are their projections on $z = 0$ planes. (a) Trajectory in spacetime with $(\sigma, P) = (0.1, 1)$. (b) Trajectory in spacetime with $(\sigma, P) = (0.001, 1)$.

equations in Linet-Tian spacetime for a few special cases [30]. In 2019, Célérier *et al.* explored radial, axial, and circular geodetic motions in a cylindrically symmetric translating spacetime [31]. In 2016, Hoseini *et al.* came up with an analytic solution to the geodesic equation in a static cylindrically symmetric conformal spacetime [32]. However, the search for a complete, exact solution to the geodetic motion of massive and massless particles moving in Levi-Civita spacetime continues to this day. This is because the differential geodesic equations it gives rise to are too complicated to solve exactly in terms of elementary[1] functions (see Appendix A). As a preview, Fig. 1 shows two typical three-dimensional trajectories of massive particles moving in Levi-Civita spacetime.

In this article, we present a complete, exact solution by quadrature to the differential geodesic equations in Levi-Civita spacetime using the Hamilton-Jacobi formalism.[2] The Hamilton-Jacobi formalism serves as a very powerful tool to solve Hamiltonian systems when the corresponding Hamilton-Jacobi equation is separable [37,38]. Interestingly enough, the Hamiltonian corresponding to the geodesic motion in Levi-Civita spacetime gives rise to a separable Hamilton-Jacobi equation and, consequently, the equation of motion is reduced to quadrature. The resulting integral solutions are also expanded into infinite series. The resulting integral solution to the geodetic motion is presented for arbitrary parameters and initial conditions; the integrations are performed for a few special cases and the results are compared to the Newtonian counterparts. A proof of a theorem on the boundedness of the orbits for both Newtonian and relativistic cases is demonstrated. Moreover, a classification of the orbits is presented based on the orbit parameters.

II. MOTION IN CYLINDRICALLY SYMMETRIC SPACETIMES

Though the metric tensor of Levi-Civita spacetime, as depicted in Eq. (1), represents the general cylindrically symmetric solution of Einstein's equation in vacuum, the geometric meaning of the coordinates used may not be immediately transparent. In particular, the radial coordinate ξ does not represent the "circumferential radius"; that is to say, when the angular coordinate ϕ goes from 0 to 2π keeping the other coordinates fixed, the proper distance covered is not equal to $2\pi\xi$. To resolve this issue, we make a coordinate transformation of the form

$$\rho = P\xi^{1-2\sigma} \tag{3}$$

keeping the other coordinates unchanged. Under the above transformation, the new metric tensor can be written as

$$\mathbf{ds}^2 = -\left(\frac{\rho}{P}\right)^{\frac{4\sigma}{1-2\sigma}}\mathbf{d}t \otimes \mathbf{d}t + \left(\frac{\rho}{P}\right)^{\frac{8\sigma^2}{1-2\sigma}}\mathbf{d}\rho \otimes \mathbf{d}\rho + \rho^2\mathbf{d}\phi \otimes \mathbf{d}\phi + \left(\frac{\rho}{P}\right)^{-4\sigma}\mathbf{d}z \otimes \mathbf{d}z. \tag{4}$$

As the angular coordinate runs from 0 to 2π, the radial coordinate ρ in Eq. (4) can be interpreted as the "circumferential radius." As it will turn out later, this choice of radial coordinate in the weak gravitational field limit facilitates establishing a correspondence between the relativistic cylindrically symmetric vacuum spacetime and its Newtonian gravitational counterpart written in cylindrical polar coordinates.

A. Motion of a massive particle

To find the solution to the geodetic motion of a point particle moving in a curved spacetime, one needs to separate the equation obtained upon substituting Eq. (B7) into Eq. (B5). The substitution results in

$$1 + g^{\mu\nu}\frac{\partial S}{\partial q^\mu}\frac{\partial S}{\partial q^\nu} = 0 \tag{5}$$

Substitution of the metric tensor from Eq. (4) yields the Hamilton-Jacobi equation for a massive particle moving in a cylindrically symmetric vacuum spacetime,

[1] *Elementary functions* are those that can be obtained in a finite number of algebraic operations, taking exponentials and logarithms [33].

[2] *Complete solution* refers to the solution to the equation of motion where the corresponding Hamilton's principal function contains the appropriate number of separation constants [34]. On the other hand, the *exact solution* means that the presented solution is neither an approximate nor a numerical one. And finally, *solution by quadrature* (also known as "reduction to quadrature") refers to the solution of a differential equation in terms of one or more definite integrals containing all of the initial data explicitly. Many differential equations in physics are solved in this manner whenever a solution in terms of elementary functions is not available [35,36].

$$1-\left(\frac{\rho}{P}\right)^{-\frac{4\sigma}{1-2\sigma}}\left(\frac{\partial S}{\partial t}\right)^2+\left(\frac{\rho}{P}\right)^{-\frac{8\sigma^2}{1-2\sigma}}\left(\frac{\partial S}{\partial \rho}\right)^2+\rho^{-2}\left(\frac{\partial S}{\partial \phi}\right)^2+\left(\frac{\rho}{P}\right)^{4\sigma}\left(\frac{\partial S}{\partial z}\right)^2=0. \tag{6}$$

Equation (6) appears to be a separable one as the coefficients are functions of ρ only. To separate the equations, we try an ansatz of the form $S(t,\rho,\phi,z)=S_t(t)+S_\rho(\rho)+S_\phi(\phi)+S_z(z)$. Upon separation, we integrate the separated equations and reconstruct the generation function as

$$S=-\Delta t+A\phi+Bz+\int\left\{\Delta^2\left(\frac{\rho}{P}\right)^{-4\sigma}-A^2\rho^{-2}\left(\frac{\rho}{P}\right)^{\frac{8\sigma^2}{1-2\sigma}}-B^2\left(\frac{\rho}{P}\right)^{\frac{4\sigma}{1-2\sigma}}-\left(\frac{\rho}{P}\right)^{\frac{8\sigma^2}{1-2\sigma}}\right\}^{\frac{1}{2}}d\rho \tag{7}$$

where Δ, A, and B are separation constants and serve as the first half of the constants of motion. It is straightforward to see that A is the conserved momentum conjugate to the azimuthal coordinate, B can be interpreted as the conserved momentum along the z coordinate, and Δ is the total energy of the moving particle.

The motion of a particle in four-dimensional spacetime contains six constants of motion, three of which we have already obtained and interpreted for their physical significance. The other constants of motion are contained in the final solution of the geodesic motion obtained through applying Eq. (B8). All of these constants are related to the initial data, namely, the initial momenta and initial coordinates. In this article, we chose the initial coordinates ρ_0, ϕ_0, and z_0, the initial momenta A and B, and the total energy Δ to appear explicitly in the final integral solution,

$$t=\Delta\int_{\rho_0}^{\rho}\left(\frac{\rho}{P}\right)^{-4\sigma}\left\{\Delta^2\left(\frac{\rho}{P}\right)^{-4\sigma}-A^2\rho^{-2}\left(\frac{\rho}{P}\right)^{\frac{8\sigma^2}{1-2\sigma}}-B^2\left(\frac{\rho}{P}\right)^{\frac{4\sigma}{1-2\sigma}}-\left(\frac{\rho}{P}\right)^{\frac{8\sigma^2}{1-2\sigma}}\right\}^{-\frac{1}{2}}d\rho, \tag{8a}$$

$$\phi=\phi_0+A\int_{\rho_0}^{\rho}\rho^{-2}\left(\frac{\rho}{P}\right)^{\frac{8\sigma^2}{1-2\sigma}}\left\{\Delta^2\left(\frac{\rho}{P}\right)^{-4\sigma}-A^2\rho^{-2}\left(\frac{\rho}{P}\right)^{\frac{8\sigma^2}{1-2\sigma}}-B^2\left(\frac{\rho}{P}\right)^{\frac{4\sigma}{1-2\sigma}}-\left(\frac{\rho}{P}\right)^{\frac{8\sigma^2}{1-2\sigma}}\right\}^{-\frac{1}{2}}d\rho, \tag{8b}$$

$$z=z_0+B\int_{\rho_0}^{\rho}\left(\frac{\rho}{P}\right)^{\frac{4\sigma}{1-2\sigma}}\left\{\Delta^2\left(\frac{\rho}{P}\right)^{-4\sigma}-A^2\rho^{-2}\left(\frac{\rho}{P}\right)^{\frac{8\sigma^2}{1-2\sigma}}-B^2\left(\frac{\rho}{P}\right)^{\frac{4\sigma}{1-2\sigma}}-\left(\frac{\rho}{P}\right)^{\frac{8\sigma^2}{1-2\sigma}}\right\}^{-\frac{1}{2}}d\rho. \tag{8c}$$

However, one might choose to write the solution by quadrature above in terms of Γ, the initial value of the momentum conjugate to the radial coordinate, using the relation

$$\Gamma=\left\{\Delta^2\left(\frac{\rho_0}{P}\right)^{-4\sigma}-A^2\rho_0^{-2}\left(\frac{\rho_0}{P}\right)^{\frac{8\sigma^2}{1-2\sigma}}-B^2\left(\frac{\rho_0}{P}\right)^{\frac{4\sigma}{1-2\sigma}}-\left(\frac{\rho_0}{P}\right)^{\frac{8\sigma^2}{1-2\sigma}}\right\}^{\frac{1}{2}} \tag{9}$$

instead of Δ.

In that case, Δ should be written in terms of Γ and the other constants of motion.

The solution by quadrature given in Eqs. (8a)–(8c) includes nonelementary integrals, which can be integrated numerically for the general cases if needed. Nevertheless, for the case of $A=0$ along with $B=0$, the angular and axial equations reduce to $\phi=\phi_0$ and $z=z_0$, respectively, implying a purely radial motion. The only nontrivial integral is that of t, which can be performed using the Euler-Gauss hypergeometric function ${}_2F_1$ [39], giving t as a function of ρ in a closed form,[3]

$$t=\frac{P}{1-2\sigma}\left[\left(\frac{\rho}{P}\right)^{1-2\sigma}{}_2F_1\left(\frac{1}{2},\frac{1-4\sigma+4\sigma^2}{4\sigma};\frac{1+4\sigma^2}{4\sigma};\frac{1}{\Delta^2}\left(\frac{\rho}{P}\right)^{\frac{4\sigma}{1-2\sigma}}\right)\right]_{\rho_0}^{\rho}. \tag{10}$$

In addition, it can be easily checked that, in the limit $\sigma\to 0$ and $P=1$, Eqs. (8a)–(8c) boils down to the geodesic equations of a massive particle moving in a flat spacetime written in cylindrical polar coordinates. Moreover, in the case of $\sigma\to 0$ but $P\neq 1$, the geodetic motion reduces to the motion on a "hypercone," i.e., the three-dimensional analog of a conical surface.

B. Null geodesics

Not unlike a massive particle, a massless particle parallel transports its four-momentum along with its worldline. Upon integration, this leads to the constraint (B6), which determines the trajectory of the massless particle. The set of all possible trajectories through a point constitutes a hypersurface in four-dimensional spacetime, known as the light cone. The light cone imposes a physical limit on the trajectories of all particles such that no causal geodesic can reside outside of it. Since a massive cosmic

[3]Using the identity $\int\frac{1}{\sqrt{1-x^n}}dx=x\cdot{}_2F_1(\frac{1}{2},\frac{1}{n};1+\frac{1}{n};x^n)$.

string might be able to strongly bend light that is intense enough to observe, obtaining the photon trajectories is therefore of particular interest. The same procedure used for the massive particles (Sec. II A), when deployed for the massless ones, leads to a generating function for the Hamilton-Jacobi equation, giving rise to the massless particle trajectories. Like the massive particle case, the motion of a massless particle includes six constants of integration, namely, Δ, A, B, and the initial coordinates ρ_0, ϕ_0, and z_0,

$$t = \Delta \int_{\rho_0}^{\rho} \left(\frac{\rho}{P}\right)^{-4\sigma} \left\{ \Delta^2 \left(\frac{\rho}{P}\right)^{-4\sigma} - A^2\rho^{-2}\left(\frac{\rho}{P}\right)^{\frac{8\sigma^2}{1-2\sigma}} - B^2\left(\frac{\rho}{P}\right)^{\frac{4\sigma}{1-2\sigma}} \right\}^{-\frac{1}{2}} d\rho, \tag{11a}$$

$$\phi = \phi_0 + A \int_{\rho_0}^{\rho} \rho^{-2}\left(\frac{\rho}{P}\right)^{\frac{8\sigma^2}{1-2\sigma}} \left\{ \Delta^2 \left(\frac{\rho}{P}\right)^{-4\sigma} - A^2\rho^{-2}\left(\frac{\rho}{P}\right)^{\frac{8\sigma^2}{1-2\sigma}} - B^2\left(\frac{\rho}{P}\right)^{\frac{4\sigma}{1-2\sigma}} \right\}^{-\frac{1}{2}} d\rho, \tag{11b}$$

$$z = z_0 + B \int_{\rho_0}^{\rho} \left(\frac{\rho}{P}\right)^{\frac{4\sigma}{1-2\sigma}} \left\{ \Delta^2 \left(\frac{\rho}{P}\right)^{-4\sigma} - A^2\rho^{-2}\left(\frac{\rho}{P}\right)^{\frac{8\sigma^2}{1-2\sigma}} - B^2\left(\frac{\rho}{P}\right)^{\frac{4\sigma}{1-2\sigma}} \right\}^{-\frac{1}{2}} d\rho. \tag{11c}$$

Similar to the massive particle case, the integral solution given in Eqs. (11a)–(11C) involves nonelementary integrals and numerical methods can be employed to perform the integrals. However, there exist a couple of special yet physically interesting cases, where the integrals can be carried out using the Euler-Gauss hypergeometric function ${}_2F_1$ introduced in Sec. II A. One of the special cases where the integrations can be performed is $B = 0$. It involves motion confined to the $z = z_0$ plane, which is significant due to its potential for aiding the direct observation of cosmic strings. On performing the integrals, t and ϕ can be expressed as functions of ρ in closed forms through the Euler-Gauss hypergeometric function,

$$t = \frac{P}{1-2\sigma}\left[\left(\frac{\rho}{P}\right)^{1-2\sigma} {}_2F_1\left(\frac{1}{2}, -\frac{1-4\sigma+4\sigma^2}{2-8\sigma}; \frac{1-4\sigma-4\sigma^2}{2-8\sigma}; \frac{A^2}{\Delta^2 P^2}\left(\frac{\rho}{P}\right)^{\frac{-2-8\sigma}{1-2\sigma}}\right)\right]_{\rho_0}^{\rho}, \tag{12a}$$

$$\phi = \phi_0 - \frac{(1-2\sigma)A}{(1-4\sigma-4\sigma^2)P\Delta}\left[\left(\frac{\rho}{P}\right)^{\frac{-1-4\sigma-4\sigma^2}{1-2\sigma}} {}_2F_1\left(\frac{1}{2}, \frac{1-4\sigma-4\sigma^2}{2-8\sigma}; \frac{3-12\sigma-4\sigma^2}{2-8\sigma}; \frac{A^2}{\Delta^2 P^2}\left(\frac{\rho}{P}\right)^{\frac{-2-8\sigma}{1-2\sigma}}\right)\right]_{\rho_0}^{\rho}. \tag{12b}$$

Another important case resulting in a solution in terms of a well-known function is that of zero angular momentum with a nonzero axial momentum, leading to the motion of a massless particle entirely confined to the plane $\phi = \phi_0$. This solution provides a graphic connection between the radial and axial motion of the particle, which, in turn, provides insights into the gravitational strength of the cosmic string. This might allow us to measure the gravitational strength of an observable cosmic string by observing the accreting photons in its local vicinity moving through gas clouds. Similar to the case of zero axial momentum, the solution to this one can also be written in a closed form using the Euler-Gauss hypergeometric function. As one might expect, both solutions to the special cases $A = 0$ [given in (12a) and (12b)] and $B = 0$ (given below) reduce to the same expression when these conditions hold simultaneously,[4]

$$t = \frac{P}{1-2\sigma}\left[\left(\frac{\rho}{P}\right)^{1-2\sigma} {}_2F_1\left(\frac{1}{2}, \frac{1-4\sigma+4\sigma^2}{8\sigma-8\sigma^2}; \frac{1+4\sigma-4\sigma^2}{8\sigma-8\sigma^2}; \frac{B^2}{\Delta^2}\left(\frac{\rho}{P}\right)^{\frac{8\sigma-8\sigma^2}{1-2\sigma}}\right)\right]_{\rho_0}^{\rho}, \tag{13a}$$

$$z = z_0 + \frac{(1-2\sigma)PB}{(1+4\sigma-4\sigma^2)\Delta}\left[\left(\frac{\rho}{P}\right)^{\frac{1+4\sigma-4\sigma^2}{1-2\sigma}} {}_2F_1\left(\frac{1}{2}, \frac{1+4\sigma-4\sigma^2}{8\sigma-8\sigma^2}; \frac{1+12\sigma-12\sigma^2}{8\sigma-8\sigma^2}; \frac{B^2}{\Delta^2}\left(\frac{\rho}{P}\right)^{\frac{8\sigma-8\sigma^2}{1-2\sigma}}\right)\right]_{\rho_0}^{\rho}. \tag{13b}$$

[4]Due to the fact that ${}_2F_1(p, q; r; 0) = 1$ for all $p, q, r \in \mathbb{N}$.

C. Series solution to the geodesic equations

The complete, exact solution by quadrature to the massive particle geodesics presented in Eqs. (8a)–(8c) and to the massless particle geodesics presented in Eqs. (11a)–(11c) is enough to extract all of the necessary information about the motion in Levi-Civita spacetime. However, one might want to explore the nature of the functions presented in Eqs. (8a)–(8c) and (11a)–(11c) to a greater extent. It will allow us to understand not only the motion in Levi-Civita spacetime but also its connection to similar motions in other settings.

In order to explore the nature of the functions in Eqs. (8a)–(8c) and (11a)–(11c), we need to expand the functions into a series. To achieve that goal, we reduce the integrals in Eqs. (8a)–(8c) and (11a)–(11c) to a common format and define it as a function $\kappa(a,b;p,q,r;x)$,

$$\begin{aligned}\kappa(a,b;p,q,r;x) &= \int_0^x (1-x^p-ax^q-bx^r)^{-\frac{1}{2}}dx \\ &= \sum_{k=0}^{\infty}\sum_{k_1,k_2,k_3}\binom{-\frac{1}{2}}{k}\frac{(-1)^k\delta^k_{k_1+k_2+k_3}a^{k_2}b^{k_3}k!}{(1+pk_1+qk_2+rk_3)k_1!k_2!k_3!}x^{1+pk_1+qk_2+rk_3}.\end{aligned} \tag{14}$$

In Eq. (14), we have expanded the integrand using multinomial expansion and performed the integration termwise, obtaining a series expansion for the function $\kappa(a,b;p,q,r;x)$. In the expansion, k, k_1, k_2, and k_3 are all positive integers and range from 0 to ∞. Furthermore, $\delta^k_{k_1+k_2+k_3}$ ensures that the relation $k = k_1+k_2+k_3$ is satisfied for each of those terms in the sum. Using the integral definition and the series expansion of $\kappa(a,b;p,q,r;x)$, one can find relevant properties of the function.

The solutions by quadrature for the massive particle geodesics in Eqs. (8a)–(8c) can easily be expressed using the definition of the $\kappa(a,b;p,q,r;x)$ function, as we show below. It is worth mentioning that both the integral expressions and the series expansions are equivalent when pursuing numerical methods to generate trajectories, and ultimately choosing one of these methods boils down to a matter of preference:

$$\begin{aligned}t = \frac{P}{1-2\sigma}\left(\frac{A}{\Delta P}\right)^{\frac{1-4\sigma+4\sigma^2}{1-4\sigma}}\Bigg[\kappa\Bigg(\frac{B^2}{\Delta^2}\left(\frac{A}{\Delta P}\right)^{\frac{8\sigma-8\sigma^2}{1-4\sigma}},\frac{1}{\Delta^2}\left(\frac{A}{\Delta P}\right)^{\frac{4\sigma}{1-4\sigma}};\cdots \\ -\frac{2-8\sigma}{1-4\sigma+4\sigma^2},\frac{8\sigma-8\sigma^2}{1-4\sigma+4\sigma^2},\frac{4\sigma}{1-4\sigma+4\sigma^2};\left(\frac{A}{\Delta P}\right)^{-\frac{1-4\sigma+4\sigma^2}{1-4\sigma}}\left(\frac{\rho}{P}\right)^{1-2\sigma}\Bigg)\Bigg]_{\rho_0}^{\rho},\end{aligned} \tag{15a}$$

$$\begin{aligned}\phi = \phi_0 - \frac{PB(1-2\sigma)}{\Delta(1-4\sigma-4\sigma^2)}\left(\frac{A}{P\Delta}\right)^{\frac{1+4\sigma-4\sigma^2}{1-4\sigma}}\Bigg[\kappa\Bigg(\frac{B^2}{\Delta^2}\left(\frac{A}{\Delta P}\right)^{\frac{8\sigma-8\sigma^2}{1-4\sigma}},\frac{1}{\Delta^2}\left(\frac{A}{\Delta P}\right)^{\frac{4\sigma}{1-4\sigma}};\cdots \\ -\frac{2-8\sigma}{1-4\sigma-4\sigma^2},-\frac{8\sigma-8\sigma^2}{1-4\sigma-4\sigma^2},-\frac{4\sigma}{1-4\sigma-4\sigma^2};\left(\frac{A}{\Delta P}\right)^{\frac{1-4\sigma-4\sigma^2}{1-4\sigma}}\left(\frac{\rho}{P}\right)^{-\frac{1-4\sigma-4\sigma^2}{1-2\sigma}}\Bigg)\Bigg]_{\rho_0}^{\rho},\end{aligned} \tag{15b}$$

$$\begin{aligned}z = z_0 + \frac{PB(1-2\sigma)}{\Delta(1+4\sigma-4\sigma^2)}\left(\frac{A}{P\Delta}\right)^{\frac{1+4\sigma-4\sigma^2}{1-4\sigma}}\Bigg[\kappa\Bigg(\frac{B^2}{\Delta^2}\left(\frac{A}{\Delta P}\right)^{\frac{8\sigma-8\sigma^2}{1-4\sigma}},\frac{1}{\Delta^2}\left(\frac{A}{\Delta P}\right)^{\frac{4\sigma}{1-4\sigma}};\cdots \\ -\frac{2-8\sigma}{1+4\sigma-4\sigma^2},\frac{8\sigma-8\sigma^2}{1+4\sigma-4\sigma^2},\frac{4\sigma}{1+4\sigma-4\sigma^2};\left(\frac{A}{\Delta P}\right)^{-\frac{1+4\sigma-4\sigma^2}{1-4\sigma}}\left(\frac{\rho}{P}\right)^{\frac{1+4\sigma-4\sigma^2}{1-2\sigma}}\Bigg)\Bigg]_{\rho_0}^{\rho}.\end{aligned} \tag{15c}$$

On the other hand, to find the series expansion of the solution for the massless particle in Eqs. (11a)–(11c), one can use the same set of equations as for the massive particles in Eqs. (15a)–(15c) except substituting $b = 0$ and $r = 0$ into $\kappa(a,b;p,q,r;x)$ appearing in the equations for t, ϕ, and z.

D. Weak gravitational field limit

Another interesting scenario one might want to explore is that when the mass parameter σ is sufficiently small, leading to a weak gravitational field. For all causal geodesics having $\sigma \ll 1$, the mass density μ in Eq. (2) can be

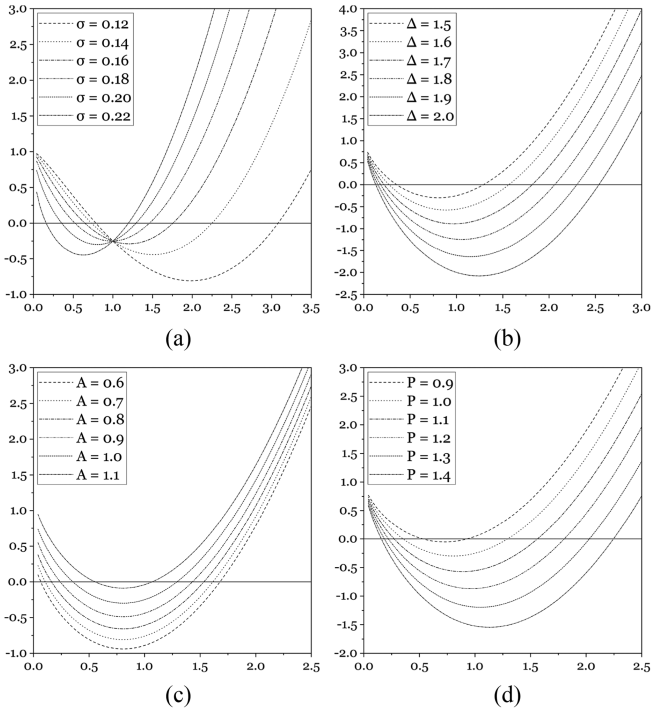

FIG. 2. $f(\rho; A, \Delta, \sigma, P)$ plots intersect the $h(\rho) = 0$ line twice, showing the existence of a lower limit $\underline{\rho}$ and an upper limit $\bar{\rho}$ of the radial coordinate. (a) Varying σ keeping $A = 1, \Delta = 1.5$, and $P = 1$. (b) Varying Δ keeping $A = 1$, $\sigma = 0.2$, and $P = 1$. (c) Varying A keeping $\Delta = 1.5, \sigma = 0.2$ and $P = 1$. (d) Varying P keeping $A = 1, \Delta = 1.5$, and $\sigma = 0.2$.

approximated as $\mu \approx \frac{\sigma}{1-2\sigma}$, since the parameter σ is bounded by $1/2$ from above in such cases. As a result, the Newtonian gravitational potential Φ for an infinitely long linear mass distribution can be written as

$$\Phi = \frac{2\sigma}{1-2\sigma}\ln\left(\frac{\rho}{R}\right), \tag{16}$$

where the linear mass density μ is approximated as mentioned above and $\rho = R$ is the surface on which the gravitational potential is taken to be zero, for an arbitrarily chosen R.

On the other hand, the metric tensor itself can be interpreted as the potential for the general-relativistic case. To see a connection between the Newtonian gravitational potential and the metric tensor in general relativity, one might expand $\mathbf{ds}^2(\mathbf{e}_t, \mathbf{e}_t)$ considering the weak gravitational field limit, where $\mathbf{e}_t$ is the coordinate basis vector along the coordinate t. Upon expansion, $\mathbf{ds}^2(\mathbf{e}_t, \mathbf{e}_t) \approx -(1 + 2\Phi)$ is expected, ignoring the second- and higher-order corrections [40]. Considering the metric tensor in Eq. (4), we write

$$\mathbf{ds}^2(\mathbf{e}_t, \mathbf{e}_t) = -\left[1 + \frac{4\sigma}{1-2\sigma}\ln\left(\frac{\rho}{P}\right) + \frac{1}{2}\left\{\frac{4\sigma}{1-2\sigma}\ln\left(\frac{\rho}{P}\right)\right\}^2 + \cdots\right]. \tag{17}$$

The quadratic and higher-order terms can be ignored as $\frac{4\sigma}{1-2\sigma} \approx 4\sigma$ in the limit $\sigma \to 0$. Indeed, it can be seen that $\mathbf{ds}^2(\mathbf{e}_t, \mathbf{e}_t) \approx -(1 + 2\Phi)$ if we choose $R = P$. This correspondence allows us to interpret P, the parameter related to the "deficit angle" of the Levi-Civita spacetime, to be the radius of the cylindrical surface on which the Newtonian gravitational potential is taken to be zero.

As demonstrated above, for small σ, there exists a correspondence between the Levi-Civita spacetime and the Newtonian gravitational field generated by an infinitely long straight mass distribution. Consequently, the respective motions of a massive particle coincide as well, in the appropriate limit, i.e., $\sigma \ll 1$.

III. BOUNDEDNESS OF ORBITS

Long before the birth of general relativity, Newton found the exact solution to the motion of a bounded point particle moving in spherically symmetric Newtonian gravity to be an ellipse, consistent with Kepler's empirical laws of planetary motion. A key insight for all of the bounded orbits, including those in Schwarzschild geometry, is that the radial coordinates describing the motions are always bounded between a minimum and a maximum value. Extending a similar investigation for the geodetic motion in Levi-Civita spacetime, we have seen that the radial coordinate ρ describing the motion is bounded between a lower limit $\underline{\rho}$ and an upper limit $\bar{\rho}$ as well. To show this, we rewrite Eq. (6) in terms of conserved momenta and set $B = 0$ to get the equation in the $z = z_0$ plane. In addition, we set the radial velocity to zero and obtain

$$\rho^2 - \Delta^2\rho^2\left(\frac{\rho}{P}\right)^{-\frac{4\sigma}{1-2\sigma}} + A^2 = 0, \tag{18}$$

which determines the extrema of the radial coordinate. This is a transcendental equation, which can be solved either graphically or numerically. To graphically see that the radial coordinate ρ is bounded between a lower limit and an upper limit, we plot the function f, defined by $f(\rho; A, \Delta, \sigma, P) := \rho^2 - \Delta^2\rho^2(\rho/P)^{-\frac{4\sigma}{1-2\sigma}} + A^2$, against ρ with physically attainable parameter values and a horizontal line defined by $h(\rho) = 0$.

In Fig. 2, apparently Eq. (18) has two distinct solutions given by the intersection points between the plots of $f(\rho; A, \Delta, \sigma, P)$ and $h(\rho)$.

On the other hand, it is instructive to find numerical solutions to Eq. (18) and obtain $\underline{\rho}$ and $\bar{\rho}$. To obtain the lower limit $\underline{\rho}$, we rewrite Eq. (18) as $\rho = \frac{A}{\sqrt{\Delta^2(\rho/P)^{-\frac{4\sigma}{1-2\sigma}} - 1}}$ and apply the fixed-point iteration technique to obtain an approximate solution for $\underline{\rho}$, using ρ_0 as the initial value solution. This is because, for the fixed-point iteration technique, $\underline{\rho}$ is a fixed point, i.e., a stable point and for any initial value that lies between $\underline{\rho}$ and $\bar{\rho}$ the iteration converges to $\underline{\rho}$. However,

for $\bar{\rho}$, this method fails as the iteration diverges away from the point. In such a case, other iteration techniques, such as the secant method, can be employed.

A. Absence of unbounded solution

A key feature of the Levi-Civita spacetime is that the orbit of a massive point particle is always bounded, unlike the trajectory in Schwarzschild spacetime. This can be proven quite generally from the fact that the function $f(\rho; A, \Delta, \sigma, P)$ increases unboundedly as the radial coordinate increases and has only one minimum, while no maximum occurs except at $\rho = 0$. Therefore, for all physically valid values of A and Δ, Eq. (18) always has two distinct solutions, $\underline{\rho}$ and $\bar{\rho}$ (excepting the circular orbits where $\underline{\rho} = \bar{\rho}$), and the radial coordinate oscillates between these two points. This proves that the radial coordinate is always bounded from above by $\bar{\rho}$, leading to a bounded orbit of a massive particle for all physically valid initial conditions.

This behavior persists in the orbit of a massive particle moving in a Newtonian gravitational field, generated by an infinitely long linear mass distribution. As can be seen from Eq. (16), the potential Φ also increases unboundedly due to its logarithmic nature. For this reason, a particle moving in it would require an infinite amount of energy to escape from the gravitational pull.

IV. CLASSIFICATION OF ORBITS

Even though the motion of a massive particle confined to the plane $z = z_0$ is significant for astrophysical observations, the solution for this case in terms of elementary functions is yet to be found. This is why it is worth resorting to numerical procedures. However, it is difficult to extract general characteristics of orbits from numerical solutions, which could have been readily found from a complete, exact solution expressed in terms of well-known functions if they were available. To mitigate the situation, we need to categorize the orbits depending on their properties. The goal of this section is to categorize different orbits based on their visual appearances and lay out a system that assigns a set of unique identification parameters to each type of orbit. To identify an orbit uniquely, only three real numbers (C, ϵ, γ) are required, which we demonstrate in Sec. IV A. Based on these parameters, we lay out a detailed categorization scheme in Sec. IV B.

A. Background of the classification scheme

Point particles moving in Schwarzschild spacetime follow precessing elliptical orbits [41]. This is formally shown in Appendix C. As proven earlier, orbits of massive point particles in Levi-Civita spacetime are also bounded between the periastron at $\rho = \underline{\rho}$ and the apastron at $\rho = \bar{\rho}$; thus, one might hypothesize that their planar geodetic motion can be approximated to be precessing ellipses as well. In order to see this, we make a number of apt approximations to Eq. (8b) considering $B = 0$, $\sigma \ll 1$, and $|\underline{\rho}/\rho| < 1$. Beginning with the integral in Eq. (8b) with $B = 0$, we expand the integrand retaining up to quadratic terms in both σ and $|\underline{\rho}/\rho|$. This allows us to perform the integration, resulting in the following closed-form formula for trajectory in the $z = z_0$ plane:

$$\left(\frac{\rho}{\underline{\rho}}\right)^{1-\eta} = \frac{C}{1 - \epsilon\cos[\gamma(\phi - \delta)]}, \tag{19}$$

where C, ϵ, γ, and δ are dimensionless quantities (given by the formulas below) that carry information about the size, eccentricity, precession rate, and phase shift of the orbit. These parameters are dependent on the initial conditions. On the other hand, the parameter η is dependent on the spacetime itself. For Levi-Civita spacetime, it is $\eta = 2\sigma + 8\sigma^2$,

$$C = \left[4\sigma\underline{\rho}^2 + 8\sigma^2A^2 + 24\sigma^2\underline{\rho}^2 + 16\sigma^2\underline{\rho}^2\ln\left(\frac{\underline{\rho}}{P}\right)\right]^{-1} \times \left[A^2 + 2\sigma\underline{\rho}^2 + 4\sigma A^2\ln\left(\frac{\underline{\rho}}{P}\right) + 12\sigma^2A^2 + 16\sigma^2\underline{\rho}^2 + 8\sigma^2A^2\ln\left(\frac{\underline{\rho}}{P}\right) + 8\sigma^2\underline{\rho}^2\ln\left(\frac{\underline{\rho}}{P}\right) + 8\sigma^2A^2\ln^2\left(\frac{\underline{\rho}}{P}\right)\right], \tag{20a}$$

$$\epsilon = \left[4\sigma\underline{\rho}^2 + 24\sigma^2\underline{\rho}^2 + 8\sigma^2A^2 + 16\sigma^2\underline{\rho}^2\ln\left(\frac{\underline{\rho}}{P}\right)\right]^{-1} \times \left[\Delta^2A^2\underline{\rho}^2 - A^2\underline{\rho}^2 + 2\sigma\Delta^2\underline{\rho}^4 - 2\sigma\underline{\rho}^4 - 6\sigma A^2\underline{\rho}^2 + 4\sigma\Delta^2A^2\underline{\rho}^2\ln\left(\frac{\underline{\rho}}{P}\right) + 4\sigma\Delta^2A^2\underline{\rho}^2\ln\left(\frac{\underline{\rho}}{P}\right) - 8\sigma A^2\underline{\rho}^2\ln\left(\frac{\underline{\rho}}{P}\right) - 4\sigma^2A^4 + 16\Delta^2\underline{\rho}^4\sigma^2 - 12\underline{\rho}^4\sigma^2 + 12\Delta^2\sigma^2A^2\underline{\rho}^2 - 44\sigma^2A^2\underline{\rho}^2 + 8\Delta^2\sigma^2\underline{\rho}^4\ln\left(\frac{\underline{\rho}}{P}\right) - 16\sigma^2\underline{\rho}^4\ln\left(\frac{\underline{\rho}}{P}\right) + 8\Delta^2\sigma^2A^2\underline{\rho}^2\ln\left(\frac{\underline{\rho}}{P}\right) - 64\sigma^2A^2\underline{\rho}^2\ln\left(\frac{\underline{\rho}}{P}\right) + 8\Delta^2\sigma^2A^2\underline{\rho}^2\ln^2\left(\frac{\underline{\rho}}{P}\right) - 32\sigma^2A^2\underline{\rho}^2\ln\left(\frac{\underline{\rho}}{P}\right)\right]^{\frac{1}{2}}, \tag{20b}$$

$$\gamma = \left[\frac{1-4\sigma-4\sigma^2}{1-2\sigma}\right] \times \left[1 + 2\sigma\frac{\rho^2}{A^2} + 12\sigma^2 + 16\sigma^2\frac{\rho^2}{A^2} - 8\sigma^2 \ln\left(\frac{\rho}{P}\right)\right]^{\frac{1}{2}}, \tag{20c}$$

$$\delta = \phi_0 - \frac{1}{\gamma}\arccos\left[\frac{1}{\epsilon} - \frac{C}{\epsilon}\left(\frac{\rho}{\rho_0}\right)^{1-\eta}\right]. \tag{20d}$$

It is evident from Eq. (19) that the trajectory approximately follows a precessing elliptical orbit. We also notice that the shape of the trajectory is uniquely determined by only three of the parameters, namely C, ϵ, and γ. This is because the parameter δ can always be set to zero by a mere rotation with respect to the z axis.

The parameter C determines the size of the orbit. An important thing to notice in Eq. (20a) is that C goes to infinity as σ approaches zero. This is reasonable since $\sigma = 0$ represents the complete absence of the matter distribution, leading to a straight-line trajectory. Another important parameter characterizing the orbit is its eccentricity ϵ, such that $0 \leq \epsilon < 1$ for a spacetime with a nonzero σ. In such a spacetime, the orbit of a massive particle is always bounded between $\rho = \underline{\rho}$ and $\rho = \bar{\rho}$, as we proved in Sec. III A. From this, one concludes that the orbit must have an eccentricity that is always less than 1.

Out of the four parameters of the trajectory, γ is the most important one for our purpose since it determines the rate of precession and consequently the number of "petals." However, for a closed orbit, γ must be a rational number. For an irrational γ, the orbit never closes and the trajectory keeps filling out a circular area as time increases. Hence, simply counting the number of "petals" loses its meaning. In Sec. IV B, we lay out a classification scheme that is practical and incorporates all possible orbits.

B. Classification scheme

It is apparent from Eq. (20) that the parameters C, ϵ, and γ contain all of the information regarding an orbit in the $z = z_0$ plane. The parameter C defines the size of the orbit, and the parameter ϵ defines the eccentricity of the orbit. A rather interesting one is the parameter γ. Depending on its value, an orbit can be a closed or an ever-precessing one. Tweaking its value, one can even change the number of "petals" in a closed orbit. Figure 3 shows two examples of possible orbits of massive particles in Levi-Civita spacetime. The first one is a closed orbit with three petals and the second one is a precessing orbit with six petals. Therefore, given enough time ($t \approx 28\,300$), the trajectory will start to fill the localized region between $\underline{\rho}$ and $\bar{\rho}$. Before discussing the categorization scheme, we need to define a few terms.

Let us use the orbits shown in Fig. 4 as specimens to aid our discussion. Both orbits have what we call three "leaves" or "petals." To demonstrate, we number the petals of the closed orbit in Fig. 4(a), starting from 0 in the counterclockwise direction. In Fig. 4(b), a three-petal orbit is precessing and we plot three complete traces of the orbit. We call each trace a "corolla" and number them starting from 0, based on their chronology. In the diagram, the solid, the dashed, and the dotted lines represent corolla 0, corolla 1, and corolla 2, respectively. This procedure of assigning an ordered pair of numbers to identify a petal of a corolla can be generalized to any such orbits, as is done in Fig. 5(a). The first number of the pair denotes the corolla and the second denotes the petal in that corolla. We call the petals that share the same corolla [e.g., (1, 0) and (1, 2)] "sisters" and petals that share the same second number [e.g., (1, 1) and (2, 1)] "clones" of each other.

At this point, it is natural to ask for a criterion that makes the distinction between sister petals and their clones.

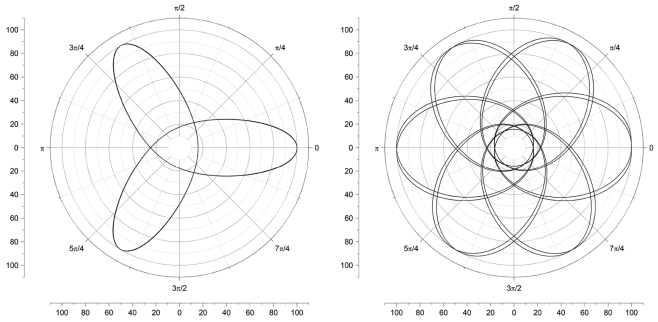

FIG. 3. Particle moving in Levi-Civita spacetime exhibiting closed and precessing trajectories. (a) A closed orbit with three petals in spacetime with $(\sigma, P) = (0.001, 1)$. (b) A precessing orbit with six petals in spacetime with $(\sigma, P) = (0.1, 1)$.

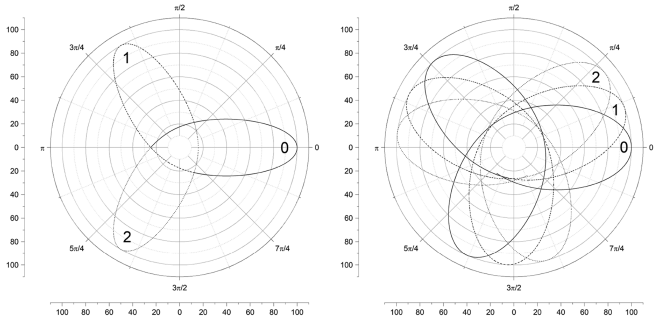

FIG. 4. A closed and a precessing orbits with three petals. (a) A corolla with three petals of a closed orbit. (b) Three corollas of a precessing orbit.

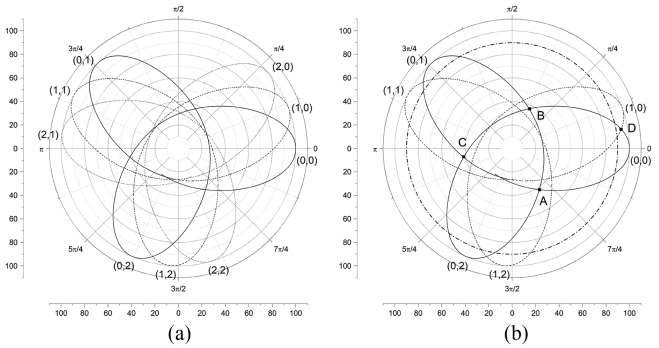

FIG. 5. Identification of a corolla in a precessing orbit. (a) Scheme for numbering petals in an orbit. (b) Distinguishing sister petals from their clones.

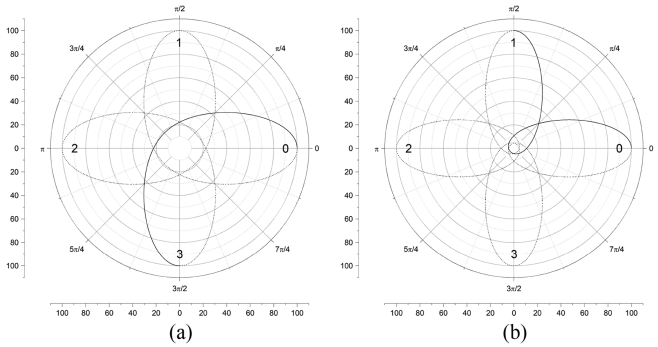

FIG. 6. Closed orbits with four petals. (a) $\gamma = 4/3$. (b) $\gamma = 4/5$.

Our definition goes like this. If, for a set of chronologically consecutive petals, all of the intersection points between any two petals fall inside of a circle defined by $\rho = \lambda\bar{\rho}$, for some $\lambda \in [0, 1]$, the petals are sisters for that chosen λ. The maximal set of sister petals makes a corolla. A petal in a corolla is said to be a clone of a petal in a preceding corolla if the mentioned petals share an intersection point that lies the farthest from the origin, among all of the intersection points in the said consecutive corollas.

For instance, in Fig. 5(b) we chose $\lambda = 0.9$, and therefore the corresponding circle $\rho = \lambda\bar{\rho}$ (dash-dotted curve) in the figure portrays a circle with a radius of 90% of the peak radial coordinate $\bar{\rho}$. In the figure, the orbit starts with the petal (0, 0), which is then followed by the petals (0, 2) and (0, 1). This three petals are sisters, as any intersection point (for example, the points A, B, and C) between these petals remains inside the dash-dotted circle. The set of (0, 0), (0, 1), and (0, 2) also make a corolla, as the chronologically fourth petal (1, 0) has an intersection point (point D) that falls outside of the dash-dotted circle. In Fig. 5(b), since D is the farthest from the origin among all of the intersection points, the petal (1, 0) is a clone of (0, 0).

Finally, armed with a precise definition of a corolla, we are ready to lay out the desired categorization scheme. We split the orbit parameter γ in Eq. (19) such that

$$\gamma = \frac{m - \chi}{n} \tag{21}$$

where m and n are positive coprime integers and χ is a real number on the interval $(-1, 1)$. A quick inspection reveals that m is the number of petals in a corolla, n is the "winding number," i.e., the number of complete rotations a massive particle makes around the cosmic string during the course of a single corolla, and χ is a small number that represent the "rate of precession" of a corolla. If $\chi = 0$ for the orbit, we refer to its corolla as "closed," meaning that it is not precessing. It is worth mentioning that an orbit with a closed corolla is always closed, but the converse is not true. Evidently, the numbers m, n, and χ for a given orbit depend on, but are not sensitive to, the choice of λ.[5] We discuss the dependence of the orbit parameters on the parameter λ in detail in Appendix D.

Throughout this article, we have chosen $\lambda = 0.9$. One can pick a higher or a lower value of λ for convenience. To avoid ambiguity, one must mention the λ parameter of their classification scheme. For example, we call our classification scheme a "90% level classification scheme."

In Fig. 6, both orbits have closed corollas with four petals each, as they have $m = 4$. However, the one in Fig. 6(a) makes three full rotations around the center before it reaches its initial position as it has $n = 3$. Right after leaving the petal 0, the particle in Fig. 6(a) skips two petals and traces out petal 3 directly. On the other hand, the orbit in Fig. 6(b) has $n = 5$ and makes five full rotations before reaching the initial position. After leaving petal 0, the particle makes a full rotation around the center and reaches petal 1. In the course of going from petal 0 to petal 1, the particle skips four petals. It is impossible to have an orbit of four petals in which the particle skips one petal after leaving petal 0 and enters petal 2 directly because, in that situation, the particle would enter petal 0 after leaving petal 2, which would make it a closed orbit of two petals only.

Similarly, in Fig. 7 all of the orbits have $m = 5$ and therefore have five petals each. However, they differ in n. The orbits in Figs. 7(a)–7(c) have $n = 4$, $n = 7$, and $n = 9$, respectively. We observe that, for any orbit, right after leaving petal 0, the particle directly enters in and traces out petal n mod m.

There is one more property that could make two closed orbits visually different: the number of extra full rotations the particle makes during the transition from one petal to another. Both particles in Figs. 7(a) and 7(c) enter petal 4 after leaving petal 0. But the particle in Fig. 7(c) makes an extra 2π rotation around the center before entering petal 4. It can be easily seen that the number of

[5]A finitely small change in λ results in a finitely small change in the orbit parameters [42].

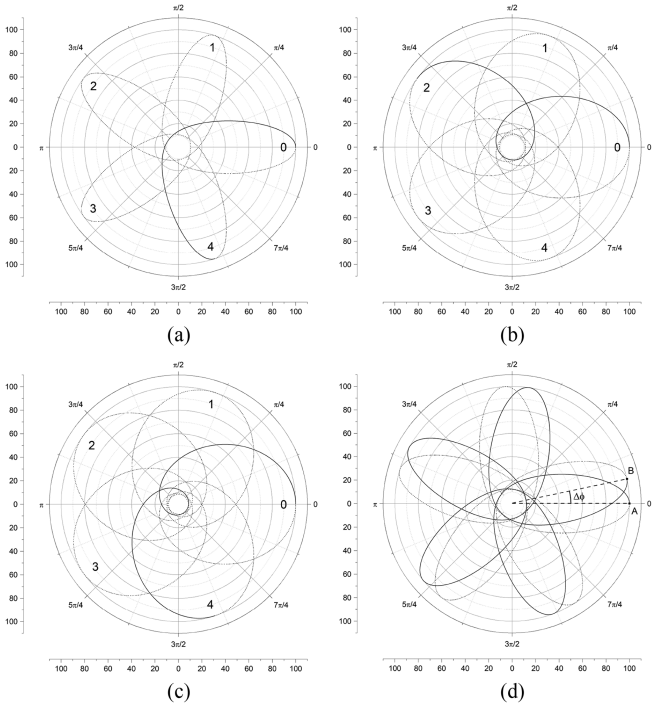

FIG. 7. Orbits with five petals. (a) $\gamma = 5/4$. (b) $\gamma = 5/7$. (c) $\gamma = 5/9$. (d) $\gamma \approx \frac{1}{4}(5 - 0.0413065)$.

extra full rotations w is related to m and n by the relation $n = (w+1)m + n \bmod m$.

Finally, consider the orbit in Fig. 7(d). The orbit is, essentially, that in Fig. 7(a) with a small precession. Starting at point A, the particle traces out five petals and ends up at point B, creating an angular separation $\Delta\phi$ with its starting point A. For any orbit, one can show that the angular separation is related to the parameter χ by the relation

$$\Delta\phi = \frac{2\pi n}{m - \chi}\chi \tag{22}$$

using Eqs. (19) and (21). For an orbit, a parameter $\chi = 0$ leads to a zero angular separation between the end points, leaving a closed trace. Therefore, the parameter χ measures how badly a corolla in a given orbit fails to close.

So far, we have discussed the geometric interpretations of the parameters C, ϵ, m, n, and χ. These parameters are sufficient to identify any orbit around an infinitely long, straight cosmic string. Therefore, in our classification scheme, we assign a unique quintuple $(C, \epsilon, m, n, \chi)$ to each orbit. One might suppress the first two numbers and write the triplet (m, n, χ) only if the size and eccentricity of the orbits are not the parameters of interest.

The classification scheme we have laid out here is inspired by the 2008 work of Levin and Perez-Giz [43]. In their article, Levin and Perez-Giz laid out a scheme that categorizes the orbits around a black hole according to the geometric shapes of the orbits. They used three numbers, z, w, and v, to identify "zoom" or the number of petals, "whirl" or the extra complete rotations per petal the particle makes, and the petal number that the particle hits right after leaving petal 0, respectively. It is apparent from the discussions above that the parameters for closed orbits (z, w, v) by Levin and Perez-Giz are related to our parameters m and n by the relations

$$z = m, \tag{23a}$$

$$w = \frac{1}{m}(n - n \bmod m) - 1, \tag{23b}$$

$$v = n \bmod m. \tag{23c}$$

Equations (23a)–(23c) show that only two parameters are enough to express the information contained in the parameters z, w, and v. Another limitation of the classification scheme developed by Levin and Perez-Giz is that it would label two visually similar orbits far from each other. For example, the orbits in Figs. 7(a) and 7(d) have $\gamma \approx 1.25$ and $\gamma \approx 1.2396734$, respectively. The classification scheme of Levin and Perez-Giz would label the first one as (5, 0, 4) and the second one as (6198367, 0, 1198367). It is also prone to truncation errors. On the other hand, our classification scheme labels the orbits in Figs. 7(a) and 7(d) as (5, 4, 0) and (5, 4, 0.0413065), respectively, when the first two parameters are suppressed. For categorizing astronomically observable ellipse-like orbits, our classification scheme might prove to be useful as it labels the visually similar orbits with labels (i.e., orbit parameters) that differ by small amounts only.

V. EXAMPLES OF MASSIVE PARTICLE ORBITS

In this section, we explore the orbits of massive particles in Levi-Civita spacetime graphically. In Figs. 8–10 we see 48 orbits in total. The list includes orbits as simple as an ellipse to orbits with many petals and whirls. In these figures, the images in the first and third columns are of closed orbits, whereas those in the second and fourth columns are of orbits with small precession.

Observing the images in Figs. 8–10, we make few qualitative inferences regarding the orbit parameters. We begin our discussion by analyzing the eccentricity of the orbits. In Figs. 8(a), 8(c), and 8(e) we see three one-petal orbits with increasing winding numbers n. The orbits in the mentioned images have eccentricities 0.73, 0.738, and 0.8, respectively. This means that the orbit in Fig. 8(c) is slightly more eccentric than the one in Fig. 8(a), and the one in Fig. 8(e) is even more eccentric. Despite this, the orbit in Fig. 8(a) "looks" more eccentric than the orbits in Figs. 8(c) and 8(e). This is because the orbits in Figs. 8(c) and 8(e) make one and two extra rotations before closing. Generally, orbits with the same eccentricity but higher winding numbers look more round-shaped than those with lower n values. This behavior is seen in all of the later orbits as well.

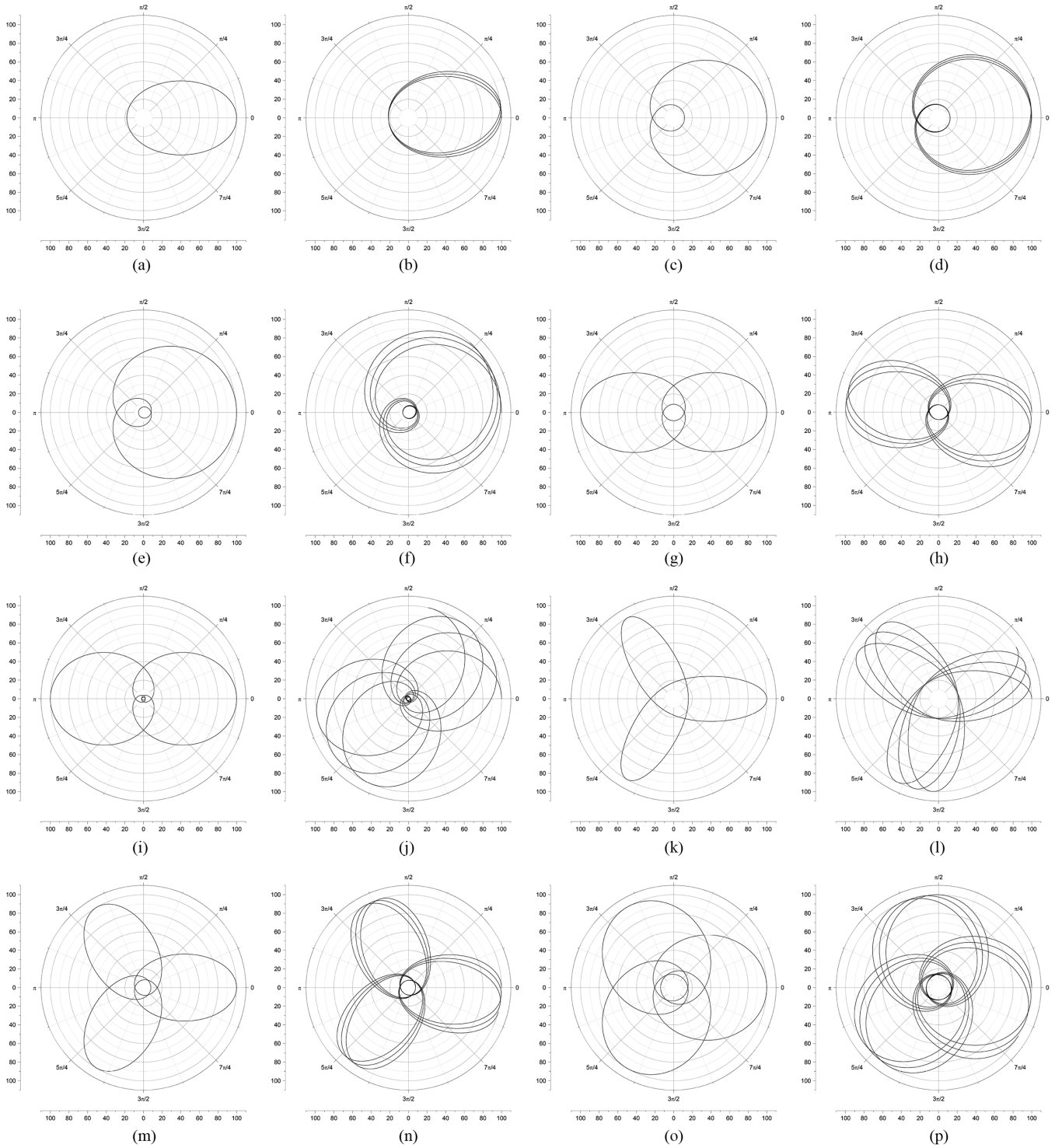

FIG. 8. Examples of massive particle orbits in Levi-Civita spacetime I. (a) $(27, 0.73, 1, 1, 0)$. (b) $(32.5, 0.675, 1, 1, 0.01024)$. (c) $(25, 0.75, 1, 2, 0)$. (d) $(26.2, 0.738, 1, 2, 0.005392)$. (e) $(20, 0.8, 1, 3, 0)$. (f) $(22, 0.78, 1, 3, 0.014784)$. (g) $(17.5, 0.825, 2, 3, 0)$. (h) $(15.8, 0.842, 2, 3, -0.013078)$. (i) $(10.3, 0.897, 2, 5, 0)$. (j) $(10.5, 0.895, 2, 5, 0.028316)$. (k) $(20.3, 0.797, 3, 2, 0)$. (l) $(28.3, 0.717, 3, 2, 0.046172)$. (m) $(14.5, 0.855, 3, 4, 0)$. (n) $(14, 0.86, 3, 4, -0.010714)$. (o) $(26.5, 0.735, 3, 5, 0)$. (p) $(25, 0.75, 3, 5, -0.01738)$.

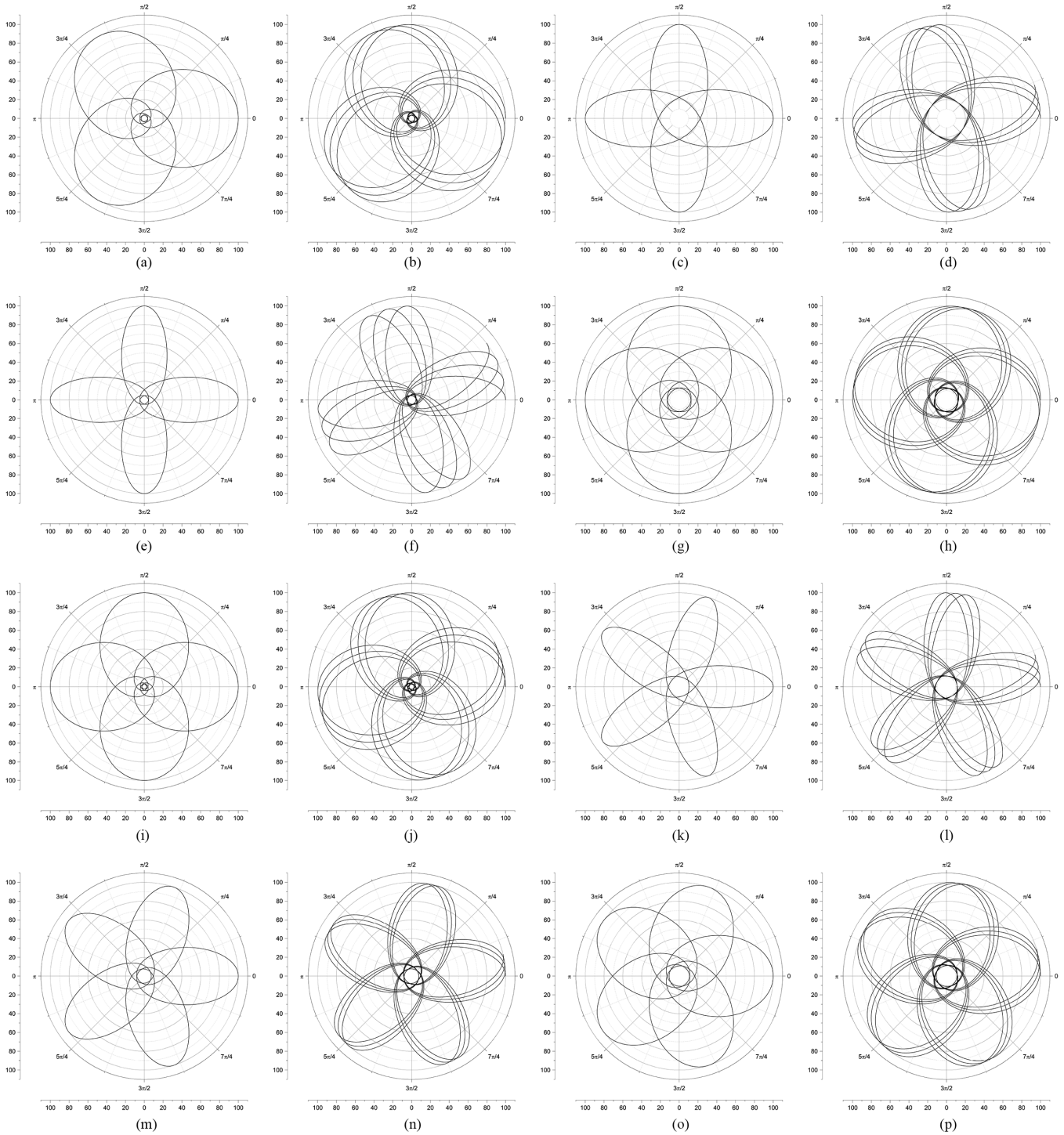

FIG. 9. Examples of massive particle orbits in Levi-Civita spacetime II. (a) $(13.1, 0.869, 3, 7, 0)$. (b) $(12.9, 0.871, 3, 7, -0.01365)$. (c) $(25.4, 0.745, 4, 3, 0)$. (d) $(28.5, 0.715, 4, 3, 0.02556)$. (e) $(7.5, 0.925, 4, 5, 0)$. (f) $(8, 0.92, 4, 5, 0.027323)$. (g) $(23.7, 0.763, 4, 7, 0)$. (h) $(23.6, 0.764, 4, 7, -0.01104)$. (i) $(11, 0.89, 4, 9, 0)$. (j) $(11.1, 0.889, 4, 9, 0.011752)$. (k) $(13.5, 0.865, 5, 4, 0)$. (l) $(14.8, 0.852, 5, 4, 0.022983)$. (m) $(12.6, 0.874, 5, 6, 0)$. (n) $(12.95, 0.8705, 5, 6, 0.01039)$. (o) $(19.55, 0.8045, 5, 7, 0)$. (p) $(19.7, 0.803, 5, 7, 0.011116)$.

Another general behavior of massive particle orbits in Levi-Civita spacetime that we observed is that the γ parameter of an orbit decreases as the spacetime parameter σ increases. Furthermore, increasing the initial azimuthal momentum decreases the γ parameter as well. These two behaviors are of significant interest as they can be used to generate orbits with desired numbers of petals and winding numbers.

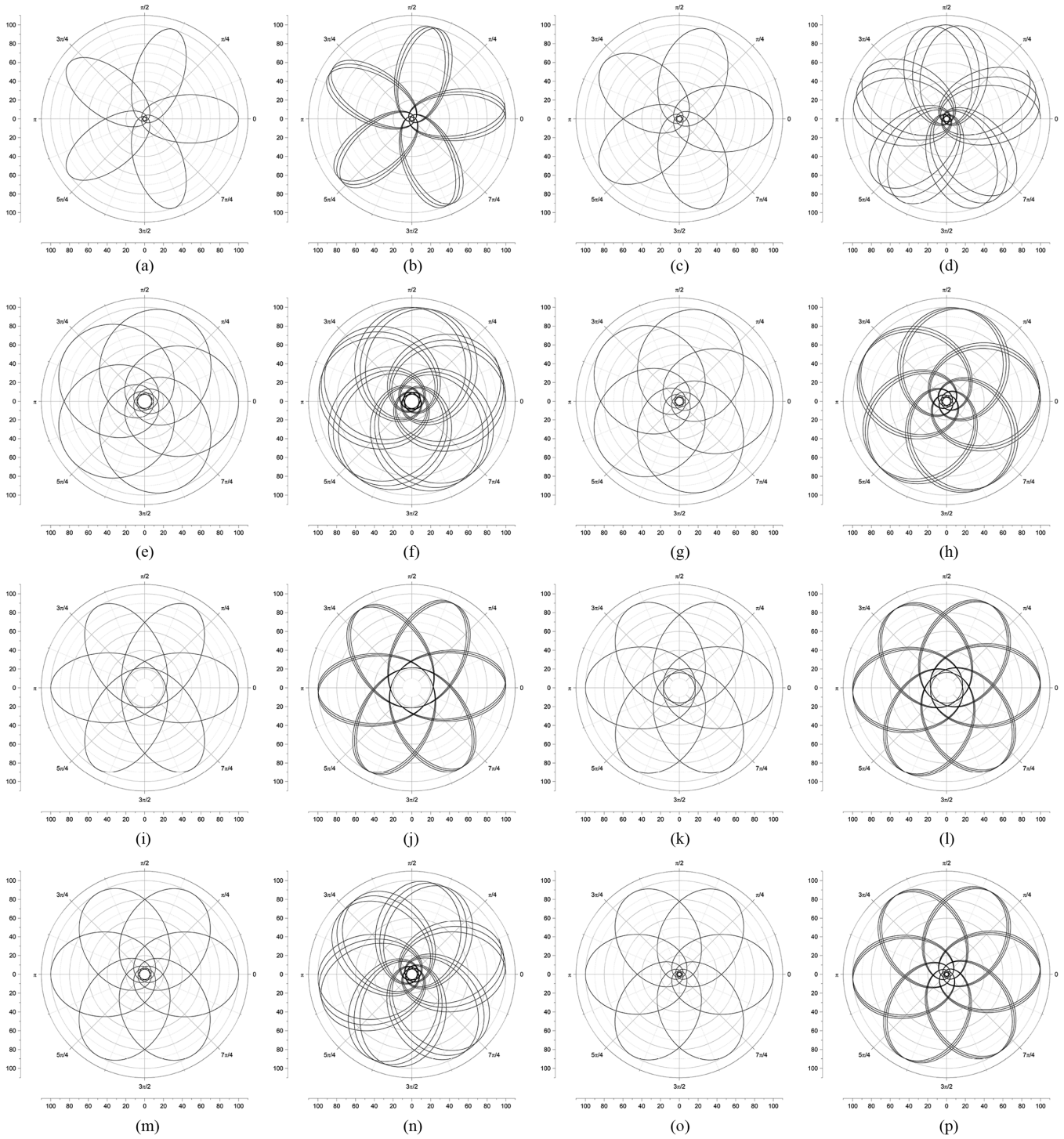

FIG. 10. Examples of massive particle orbits in Levi-Civita spacetime III. (a) $(5.4, 0.946, 5, 8, 0)$. (b) $(5.5, 0.945, 5, 8, 0.0057942)$. (c) $(8.3, 0.917, 5, 9, 0)$. (d) $(8.4, 0.916, 5, 9, 0.016061)$. (e) $(19.5, 0.805, 5, 11, 0)$. (f) $(19.4, 0.806, 5, 11, 0.011862)$. (g) $(14.7, 0.853, 5, 12, 0)$. (h) $(14.8, 0.852, 5, 12, 0.005258)$. (i) $(30.5, 0.695, 6, 5, 0)$. (j) $(30.2, 0.698, 6, 5, 0.0057664)$. (k) $(25.8, 0.742, 6, 7, 0)$. (l) $(26.1, 0.739, 6, 7, 0.005057)$. (m) $(13.8, 0.862, 6, 11, 0)$. (n) $(13.7, 0.863, 6, 11, 0.011192)$. (o) $(9.1, 0.909, 6, 13, 0)$. (p) $(9, 0.91, 6, 13, 0.0028481)$.

For an orbit with a closed corolla, a small increment of the parameter γ introduces a small clockwise precession to the orbit. This is why increasing σ or A a little bit produces a small counterclockwise precession of the orbit. One can use this property to produce closed orbits by "fine-tuning" the precessing ones.

Raising the spacetime parameter σ to a higher value leads to a sufficiently small value of γ, for which the winding

number n of an orbit is much bigger than the number of petals m of that orbit. In that situation, the particle can make one or more extra rotations around the cosmic string during its course from one petal to another. These kinds of orbits are collectively known as "zoom-whirl orbits" for their zooming and whirling behavior. For example, the orbits in Figs. 8(c) and 8(e) are single-petal zoom-whirl orbits. The zoom-whirl orbits are "strong gravity phenomena" as they require higher values of the spacetime parameter σ.

VI. COMPARISON BETWEEN NEWTONIAN AND RELATIVISTIC ORBITS

In Sec. II C, we demonstrated that the gravitational field generated by a cosmic string matches with the gravitational field of its Newtonian counterpart in the weak-field limit, $\sigma \ll 1$. In this section we explore the orbits of massive particles moving in the Newtonian gravitational field of an infinitely long linear mass distribution. We begin our discussion by deriving the complete, exact solution by quadrature to the equation of motion of a point particle around a Newtonian linear mass distribution. Considering the Newtonian gravitational potential of a linear mass distribution, we write the Hamilton-Jacobi equation for the system in cylindrical coordinates. Following the standard procedure [44], we obtain the following general integral solution to the equations of motion for the point particle:

$$t = \int_{\rho_0}^{\rho} \left\{ 2\Delta - A^2\rho^{-2} - B^2 - \frac{4\sigma}{1-2\sigma+4\sigma^2} \ln\left(\frac{\rho}{R}\right) \right\}^{-\frac{1}{2}} d\rho, \tag{24a}$$

$$\phi = \phi_0 + A \int_{\rho_0}^{\rho} \rho^{-2} \left\{ 2\Delta - A^2\rho^{-2} - B^2 - \frac{4\sigma}{1-2\sigma+4\sigma^2} \ln\left(\frac{\rho}{R}\right) \right\}^{-\frac{1}{2}} d\rho, \tag{24b}$$

$$z = z_0 + B \int_{\rho_0}^{\rho} \left\{ 2\Delta - A^2\rho^{-2} - B^2 - \frac{4\sigma}{1-2\sigma+4\sigma^2} \ln\left(\frac{\rho}{R}\right) \right\}^{-\frac{1}{2}} d\rho. \tag{24c}$$

Similar to the case of a massive particle in Levi-Civita spacetime in Eqs. (8a)–(8c), we have used the initial coordinates ρ_0, ϕ_0, and z_0, the conserved momentum conjugate to the ϕ coordinate A, the conserved momentum in the z coordinate B, and the total energy Δ as constants of motion in the final integral solution in Eqs. (24a)–(24c). However, one might want to write the integral solution in Eqs. (24a)–(24c) in terms of Γ, the initial value of the momentum conjugate to the radial coordinate, using the relation

$$\Gamma = \left\{ 2\Delta - \frac{A^2}{\rho_0^2} - B^2 - \frac{4\sigma}{1-2\sigma+4\sigma^2} \ln\left(\frac{\rho_0}{R}\right) \right\}^{\frac{1}{2}}, \tag{25}$$

instead of Δ; doing so will be useful for running numerical routines that take Γ as initial data, rather than Δ.

The Newtonian gravitational potential Φ for an infinitely long linear mass distribution is unbounded from above and goes to infinity as the radial coordinate increases, implying that the motion of a point particle around it is always bounded, like its relativistic counterpart. As a result, in the $z = z_0$ plane, the trajectory of a point particle around a Newtonian linear mass distribution always remains on a washer, defined by $\underline{\rho} < \rho < \bar{\rho}$, where $\underline{\rho}$ and $\bar{\rho}$ are the lower and upper limits of the radial coordinate, respectively. To see this, one starts with the Hamilton-Jacobi equation of the system in cylindrical coordinates and rewrites it in terms of the conserved energy Δ and conserved momenta A and B of the motion. Then, setting the momentum conjugate to the radial coordinate and B to zero, one gets

$$\frac{4\sigma}{1-2\sigma+4\sigma^2} \ln\left(\frac{\rho}{R}\right)\rho^2 - 2\Delta\rho^2 + A^2 = 0. \tag{26}$$

Equation (26) is the Newtonian analog of Eq. (18). The coordinate ρ in Eq. (26) has two distinct solutions, like its relativistic counterpart. To show this graphically, we define $g(\rho; A, \Delta, \sigma, R) := \frac{4\sigma}{1-2\sigma+4\sigma^2} \ln(\frac{\rho}{R})\rho^2 - 2\Delta\rho^2 + A^2$ and plot it against $g(\rho; A, \Delta, \sigma, R)$. In Fig. 11, we can see that the

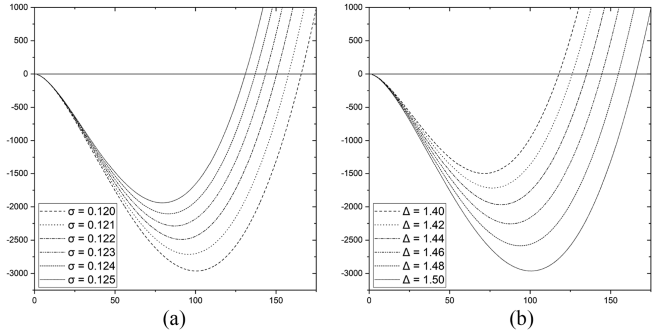

FIG. 11. $g(\rho; A, \Delta, \sigma, R)$ plots intersect the $h(\rho) = 0$ line twice, showing the existence of a lower limit $\underline{\rho}$ and an upper limit $\bar{\rho}$ of the radial coordinate. (a) Varying σ keeping $A = 1, \Delta = 1.5$, and $R = 1$. (b) Varying Δ keeping $A = 1, \sigma = 0.12$, and $R = 1$.

horizontal line $h(\rho) = 0$ intersects the curve of $g(\rho; A, \Delta, \sigma, R)$ twice, providing the two solutions to ρ. We denote the smaller solution by $\underline{\rho}$ and the larger one by $\bar{\rho}$. This establishes the fact the radial coordinate ρ is bounded between $\rho = \underline{\rho}$ and $\rho = \bar{\rho}$, as mentioned earlier in Sec. III A.

We demonstrated in Sec. IV A that, in the weak-field limit, the orbit of a massive particle in the $z = z_0$ plane in Levi-Civita spacetime approximately follows a precessing elliptical path. Naturally, the motion of a point particle around a Newtonian linear mass distribution is expected to be a precessing ellipse as well. To demonstrate this, we take Eq. (24b) and make approximations to it considering $B = 0$, $\sigma \ll 1$, and $|\underline{\rho}/\rho| < 1$, leading to the exact closed-form formula as in Eq. (19) with $\eta = 0$. The parameters of the orbit C, ϵ, γ, and δ are given by the relations

$$C = \frac{1}{4\sigma\underline{\rho}^2} \times \left[A^2 + 2\sigma\underline{\rho}^2 - 2\sigma A^2 + 4A^2\sigma^2\right], \tag{27a}$$

$$\begin{aligned}\epsilon = \frac{1}{4\sigma\underline{\rho}^2} \times \Bigg[&2\Delta A^2\underline{\rho}^2 - 8\sigma\Delta A^2\underline{\rho}^2 - 6\sigma A^2\underline{\rho}^2 \\ &+ 4\sigma\Delta\underline{\rho}^4 - 4\sigma A^2\underline{\rho}^2 \ln\left(\frac{\underline{\rho}}{R}\right) + 24\sigma^2\Delta A^2\underline{\rho}^2 \\ &+ 12\sigma^2 A^2\underline{\rho}^2 - 8\sigma^2\Delta\underline{\rho}^4 + 4\sigma^2\underline{\rho}^4 \\ &+ 8\sigma^2 A^2\underline{\rho}^2 \ln\left(\frac{\underline{\rho}}{R}\right) - 8\sigma^2\underline{\rho}^4 \ln\left(\frac{\underline{\rho}}{R}\right)\Bigg]^{\frac{1}{2}},\end{aligned} \tag{27b}$$

$$\begin{aligned}\gamma = &[1 - 2\sigma + 4\sigma^2]^{-\frac{1}{2}} \\ &\times \left[1 - 2\sigma + 2\sigma\frac{\underline{\rho}^2}{A^2} + 4\sigma^2\right]^{\frac{1}{2}},\end{aligned} \tag{27c}$$

$$\delta = \phi_0 - \frac{1}{\gamma}\arccos\left(\frac{\rho_0 - C\underline{\rho}}{\epsilon\rho_0}\right). \tag{27d}$$

As we discussed earlier for the case of massive particle orbits in Levi-Civita spacetime, the parameters C, ϵ, and γ are enough to uniquely determine the trajectory, whereas the parameter δ can always be set to zero by a rotation of coordinates around the z axis. Once again, C, ϵ, and γ contain the information regarding the size, eccentricity, and precession rate of the orbit, respectively.

However, from Eqs. (20a)–(20d) and (27a)–(27d) it is not apparent how the trajectory of a massive particle in Levi-Civita spacetime matches with the trajectory of a point mass around a Newtonian linear mass distribution in the weak-field limit. To see the correspondence, we make further approximations to Eqs. (20a)–(20d) and (27a)–(27d) considering $\sigma \ll 1$ and keep the terms containing the lowest two powers in σ. We compare the results side by side in Eqs. (28a)–(28f):

$$C_N \approx \frac{A^2}{4\sigma\underline{\rho}^2} + \frac{1}{2} - \frac{A^2}{2\underline{\rho}^2}, \tag{28a}$$

$$C_R \approx \frac{A^2}{4\sigma\underline{\rho}^2} + \frac{1}{2} - \frac{3A^2}{2\underline{\rho}^2} - \frac{A^4}{2\underline{\rho}^4}, \tag{28b}$$

$$\epsilon_N \approx \left[\frac{\Delta A^2}{8\sigma^2\underline{\rho}^2} + \frac{\Delta}{4\sigma} - \frac{3A^2}{8\sigma\underline{\rho}^2} - \frac{A^2\ln\left(\frac{\rho}{R}\right)}{4\sigma\underline{\rho}^2} - \frac{\Delta A^2}{2\sigma\underline{\rho}^2}\right]^{\frac{1}{2}}, \tag{28c}$$

$$\begin{aligned}\epsilon_R \approx \Bigg[&\frac{\tilde{\Delta}A^2}{8\sigma^2\underline{\rho}^2} + \frac{\tilde{\Delta}}{4\sigma} - \frac{3A^2}{8\sigma\underline{\rho}^2} - \frac{A^2\ln\left(\frac{\rho}{P}\right)}{4\sigma\underline{\rho}^2} - \frac{3\tilde{\Delta}A^2}{2\sigma\underline{\rho}^2} \\ &+ \frac{\tilde{\Delta}A^2\ln\left(\frac{\rho}{P}\right)}{2\sigma\underline{\rho}^2} - \frac{\tilde{\Delta}A^4}{2\sigma\underline{\rho}^4} - \frac{\tilde{\Delta}A^2\ln\left(\frac{\rho}{P}\right)}{\sigma\underline{\rho}^2}\Bigg]^{\frac{1}{2}},\end{aligned} \tag{28d}$$

$$\gamma_N \approx 1 + \sigma\frac{\underline{\rho}^2}{A^2}, \tag{28e}$$

$$\gamma_R \approx 1 + \sigma\frac{\underline{\rho}^2}{A^2} - 2\sigma, \tag{28f}$$

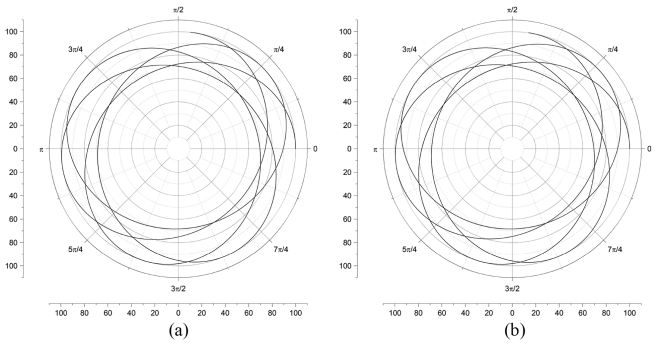

FIG. 12. Massive particle moving in Levi-Civita spacetime (left) and around a Newtonian linear mass distribution (right) with parameter $\sigma = 0.0003$. (a) $(80.8, 0.192, 3, 2, 0.1645)$. (b) $(80.8, 0.192, 3, 2, 0.1612)$.

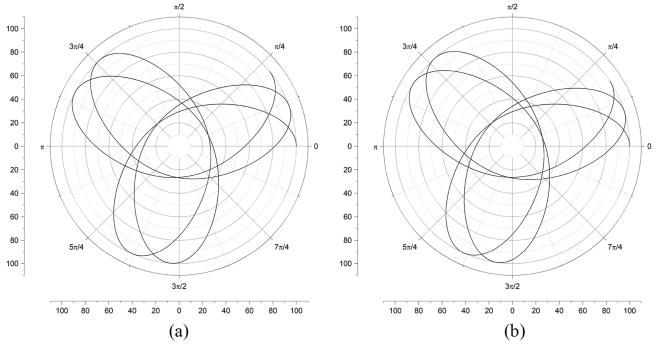

FIG. 13. Massive particle moving in Levi-Civita spacetime (left) and around a Newtonian linear mass distribution (right) with parameter $\sigma = 0.001$. (a) $(35.8, 0.642, 3, 2, 0.07999)$. (b) $(35.8, 0.642, 3, 2, 0.06868)$.

where $\tilde{\Delta}$ is defined by the relation $\tilde{\Delta} \coloneqq \frac{1}{2}(\Delta^2 - 1)$. In the equations above, the parameters of a particle's orbit around a Newtonian linear mass density are denoted by C_N, ϵ_N, and γ_N, whereas C_R, ϵ_R, and γ_R are the parameters of a massive particle's orbit in Levi-Civita spacetime. It is apparent from Eqs. (28a)–(28f) that the massive particle orbits in Levi-Civita spacetime coincide with particle orbits around a Newtonian linear mass density in the weak gravity limit, as the corresponding orbit parameters match in the lowest power of σ and start to deviate only when the terms with the second lowest power in σ are considered. Finally, let us compare the orbits graphically.

For any set of initial data, it is expected that the orbits of massive particles in Levi-Civita spacetime will match the orbits around a Newtonian linear mass distribution in the weak gravitational field limit. Figure 12 shows a particle moving in Levi-Civita spacetime (left) and a particle moving around a Newtonian linear mass distribution (right), where both particles have the same set of initial data $(\rho_0, \phi_0, z_0, \Gamma, A, B) = (100, 0, 0, 0, 2, 0)$. For both cases, the energy density parameter is set to $\sigma = 0.0001$, making strings the sources of weak gravitational fields. As we can see, both particles in Fig. 12 follow effectively the same trajectory, confirming Eqs. (28a)–(28f). However, the orbits have a small deviation in their precession parameter χ. The difference decreases even further for the weaker gravitational sources.

Keeping the set of initial data unchanged, we increase the parameter σ and set it to 0.001 in Fig. 13, which makes both orbits more eccentric. However, the difference in the χ values of the orbits becomes larger. Apparently, the χ value for the orbit around the Newtonian linear mass density changes more rapidly than that of the massive particle orbit in Levi-Civita spacetime as σ changes. In Fig. 14 the σ parameter is set to 0.003, without changing the initial data. As a result, the orbits in Fig. 14 become more eccentric. However, the orbit in Levi-Civita spacetime becomes slightly more eccentric than the other one, and the χ value continues to change more rapidly in the orbit around the Newtonian linear mass density. All of these qualitative observations are consistent with Eqs. (28a)–(28f).

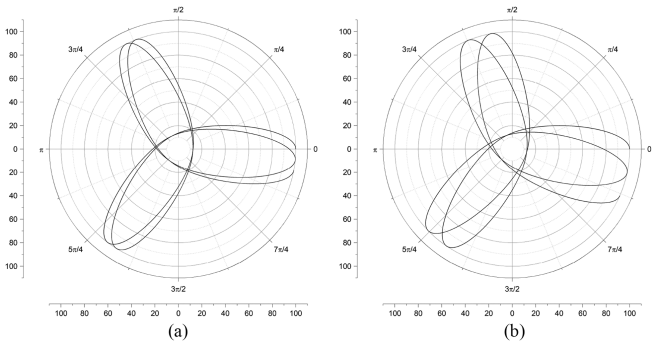

FIG. 14. Massive particle moving in Levi-Civita spacetime (left) and around a Newtonian linear mass distribution (right) with parameter $\sigma = 0.003$. (a) $(14.9, 0.851, 3, 2, 0.022021)$. (b) $(15, 0.85, 3, 2, 0.049991)$.

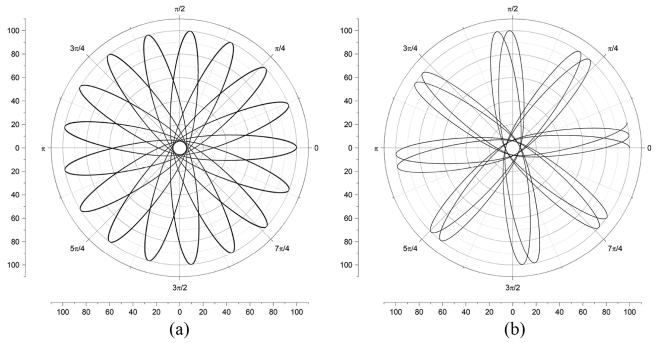

FIG. 15. Massive particle moving in Levi-Civita spacetime (left) and around a Newtonian linear mass distribution (right) with parameter $\sigma = 0.01$. (a) $(5.2, 0.948, 17, 11, 0.001294)$. (b) $(5.2, 0.948, 8, 5, 0.027502)$.

Finally, in Fig. 15 we turn up the σ parameter even further to 0.01, keeping the initial data fixed. At this point, the parameter γ of the orbits becomes different enough to break the visual similarity between the orbits.

VII. APPLICATIONS AND FUTURE WORKS

Our work potentially opens many doors for future works. Unsurprisingly, the results may have definite implications for corresponding observational works related to cosmic strings and networks of them. There is room for future theoretical works as well; for instance, further endeavours can investigate the geodetic motions confined to the $\phi = \phi_0$ plane, i.e., particles with no initial angular momentum. Similar analysis can be carried out for photon trajectories at sufficient depth. All of these works can be extended to the corresponding setting of Newtonian gravity.

The classification scheme developed in this article can now be applied to orbits in spacetimes with different characteristic symmetries, such as those of the Schwarzschild and Kerr spacetimes. Another possible extension to our work is to investigate the gravitational radiation for highly eccentric orbits of massive and massless particles around cosmic strings. Nonetheless, more pathways for future works will unfold as more work is carried out on relevant topics.

VIII. CONCLUSION

In this article, we utilized the separability of the Hamilton-Jacobi equations to derive the complete, exact integral solution to the geodesic equations for massive and massless particles in Levi-Civita spacetime. Additionally, we expanded the resulting integral solutions into corresponding infinite series. Integrals were performed to obtain solutions in terms of well-known functions for a few special cases. Moreover, the complete, exact integral solution to the Newtonian differential equation of motion for massive

particles moving around an infinitely long straight linear mass distribution was obtained as well.

A surprising discovery is that both the Newtonian and relativistic orbits are always bounded, and they coincide in the weak-field limit. Most importantly, we presented a simple classification scheme for the orbits and compared it to the other existing scheme. Finally, we applied the scheme to categorize the closed and precessing relativistic orbits of a massive particle in Levi-Civita spacetime. The relativistic massive particle trajectories were compared against their Newtonian counterparts.

ACKNOWLEDGMENTS

We would like to thank John David Brown, Prosanto Chokroborty, and Sadman Sakib for their valuable suggestions on various occasions that improved the article significantly. This material is based upon works supported by the Community of Physics.

APPENDIX A: DIFFERENTIAL GEODESIC EQUATIONS

In a four-dimensional curved spacetime, a causal geodesic is a path that a particle, whether it is massive or not, follows. During the course, a massive particle tries to maximize the proper time which, as it turns out, can be treated as the action corresponding to the motion. Therefore, extremizing the action [45]

$$\mathcal{S}[q] = \int_{\tau_i}^{\tau_f} \sqrt{-g_{\mu\nu}\dot{q}^\mu \dot{q}^\nu}\, d\tau \tag{A1}$$

leads to the geodesic equations

$$\ddot{q}^\kappa + \Gamma^\kappa_{\mu\nu}\dot{q}^\mu \dot{q}^\nu = 0, \tag{A2}$$

where the q^μ denote the spacetime coordinates, overdots denote derivatives with respect to the proper time parameter τ, and $\Gamma^\kappa_{\mu\nu}$ denote the connection coefficients of the spacetime. For the metric tensor in Eq. (4), we can find the differential geodesic equations as follows:

$$\ddot{t} + \frac{4\sigma}{(1-2\sigma)\rho}\dot{\rho}\,\dot{t} = 0, \tag{A3a}$$

$$\ddot{\rho} + \frac{2\sigma}{(1-2\sigma)P}\left(\frac{\rho}{P}\right)^{4\sigma-1}\dot{t}^2 + \frac{4\sigma^2}{(1-2\sigma)\rho}\dot{\rho}^2 - \left(\frac{\rho}{P}\right)^{-\frac{8\sigma^2}{1-2\sigma}}\rho\dot{\phi}^2 + \frac{2\sigma}{P}\left(\frac{\rho}{P}\right)^{-\frac{1+2\sigma}{1-2\sigma}}\dot{z}^2 = 0, \tag{A3b}$$

$$\ddot{\phi} + \frac{2}{\rho}\dot{\rho}\,\dot{\phi} = 0, \tag{A3c}$$

$$\ddot{z} - \frac{4\sigma}{\rho}\dot{\rho}\,\dot{z} = 0. \tag{A3d}$$

The above equations are not simple enough to solve analytically. That is why we look for another method, namely, the Hamilton-Jacobi procedure, to solve the geodesic equations.

APPENDIX B: HAMILTON-JACOBI PROCEDURE

Considering the action in Eq. (A1), we can define the Lagrangian of the system as

$$L(q, \dot{q}; \tau) = \sqrt{-g_{\mu\nu}\dot{q}^\mu \dot{q}^\nu} \tag{B1}$$

and the canonical momenta corresponding to the spacetime coordinates as

$$p_\kappa = \frac{\partial L}{\partial \dot{q}^\kappa} = -\frac{g_{\kappa\lambda}\dot{q}^\lambda}{\sqrt{-g_{\mu\nu}\dot{q}^\mu \dot{q}^\nu}}. \tag{B2}$$

Using the above definitions of the Lagrangian and the momenta, we can construct the canonical Hamiltonian of the system as

$$H(q, p; \tau) = p_\kappa \dot{q}^\kappa - L(q, \dot{q}; \tau) = 0. \tag{B3}$$

This shows that the Lagrangian of the system is degenerate, meaning the relations between the velocity and the momentum variables are not invertible. It can quite easily be shown that the determinant of the corresponding Hessian matrix is zero, confirming the degeneracy of the Lagrangian,

$$\det\left(\frac{\partial^2 L}{\partial \dot{q}^\kappa \partial \dot{q}^\lambda}\right) = 0. \tag{B4}$$

In such a case, Dirac reasoned that there exists a constraining relation between the momentum variables themselves [46]. For a massive particle, it takes the form

$$1 + g^{\mu\nu} p_\mu p_\nu = 0. \tag{B5}$$

However, for a massless particle there exists no such action principle. Rather, the constraining relation among the momenta comes from the first integral of the geodesic, which is

$$g^{\mu\nu} p_\mu p_\nu = 0. \tag{B6}$$

Together with the definition of the generating function

$$p_\mu = \frac{\partial S}{\partial q^\mu} \tag{B7}$$

Equations (B5) and (B6) can be treated as the Hamilton-Jacobi equations for the massive and massless particles, respectively [47]. The solution to the differential geodesic equations can be found using

$$Q^{\mu} = \frac{\partial S}{\partial P_{\mu}}, \tag{B8}$$

where Q^{μ} and P_{μ} are the constants of motion. For massive particles, Eq. (B5) [and for massless particles, Eq. (B6) instead] together with Eqs. (B7) and (B8) constitutes a complete set of equations from which a unique solution to the geodesics can be obtained.

APPENDIX C: CLASSIFICATION SCHEME APPLIED TO SCHWARZSCHILD SPACETIME

The classification scheme laid out in Sec. IV applies to other important spacetime geodesics as well. In particular, it aptly describes the massive particle geodesics in Schwarzschild spacetime. Even though it is well known in the literature [41], we show it systematically here for completeness. We begin with the integral solution to the orbit equation of massive particle geodesics in Schwarzschild spacetime written in Schwarzschild coordinates (t, r, θ, ϕ) (at $\theta = \pi/2$) given by the following equation:

$$\phi = \phi_0 + \int_{r_0}^{r} \frac{l}{r^2}\left\{E^2 - 1 - \frac{2M}{r} - \frac{l^2}{r^2} + \frac{2Ml^2}{r^3}\right\}^{-\frac{1}{2}} dr, \tag{C1}$$

where E is the energy of a massive particle with unit mass and l is the angular momentum of the particle [48]. We expand the integrand with respect to the periastron location $\underline{r}$ and keep the terms up to the second order in $|\underline{r}/r|$. We then integrate the approximate trajectory integral, giving an orbit equation exactly of the form depicted in Eq. (19), where the radial variable ρ is replaced by the Schwarzschild radial coordinate r with $\eta = 0$. The orbit parameters C, ϵ, γ, and δ are given by the following relations:

$$C = \frac{2k_2}{2k_2 - k_1}, \tag{C2a}$$

$$\epsilon = \sqrt{\frac{4k_0k_2 + k_1^2}{(2k_2 - k_1)^2}}, \tag{C2b}$$

$$\gamma = \frac{\underline{r}\sqrt{k_2}}{l}, \tag{C2c}$$

$$\delta = \phi_0 - \frac{1}{\gamma}\arccos\left(\frac{r_0 - C\underline{r}}{\epsilon r_0}\right). \tag{C2d}$$

In the above relations, k_0, k_1, and k_2 are defined as follows:

$$k_0 = E^2 - 1 + \frac{l^2}{4M^2} + \frac{2M}{\underline{r}} - \frac{l^2}{\underline{r}^2} + \frac{3l^2}{4M^2}\ln\left(\frac{2M}{\underline{r}}\right) + \frac{9l^2}{8M^2}\ln^2\left(\frac{2M}{\underline{r}}\right), \tag{C3a}$$

$$k_1 = -\frac{3l^2}{4M^2} - \frac{2M}{\underline{r}} + \frac{2l^2}{\underline{r}^2} - \frac{9l^2}{4M^2}\ln\left(\frac{2M}{\underline{r}}\right), \tag{C3b}$$

$$k_2 = -\frac{3l^2}{4M^2} + \frac{l^2}{\underline{r}^2} - \frac{9l^2}{8M^2}\ln\left(\frac{2M}{\underline{r}}\right). \tag{C3c}$$

Having shown that the approximate geodesic in Schwarzschild spacetime follows the path of a precessing ellipse as in Eq. (19), one can use the classification scheme laid out in Sec. IV.

APPENDIX D: DEPENDENCE OF THE ORBIT PARAMETERS ON THE PARAMETER λ

As we mentioned earlier, the orbit parameters m, n, and χ depend on, but are not sensitive to, the parameter λ. If the product $\lambda\bar{\rho}$ falls between the radial coordinate of the intersection of the two nearest sister petals and that of the two nearest clone petals, a small change in λ does not alter the orbit parameters. Mathematically, for a given λ, the orbit parameters become independent of the parameter λ on a typical interval defined by the following inequality:

$$\cos(\gamma\phi_p) < \frac{1}{\epsilon} - \frac{1-\epsilon}{\epsilon\lambda^{1-\eta}} < \cos(\gamma\phi_c). \tag{D1}$$

In the inequality above, γ is defined by Eq. (21), ϕ_p is the angular coordinate where the two nearest sister petals intersect, and ϕ_c is the angular coordinate where the two nearest clone petals intersect each other. The quantities ϕ_p and ϕ_c can be written explicitly in terms of the orbit parameters,

$$\phi_p = \frac{\pi n}{m-\chi}\left[m + 2 - \frac{m+1}{n\mathrm{mod}\ m}\right] - 2\pi\left\lfloor\frac{n}{m-\chi}\right\rfloor + \pi\left\lfloor\frac{n}{m-\chi}\left(\frac{m+1}{n\mathrm{mod}\ m} - m\right)\right\rfloor, \tag{D2a}$$

$$\phi_c = \frac{\pi n}{m-\chi}\chi. \tag{D2b}$$

However, the orbit parameters m, n, and χ change at the boundaries of the inequality in Eq. (D1). Basically, when the circle defined by the radius $\lambda\bar{\rho}$ includes or excludes an intersection point of two nearby petals on the trajectory due to a small change in λ, the orbit parameters change. In fact, on a given orbit, there are many such intervals inside which the orbit parameters are independent of the variation of λ. The boundaries of those intervals, where small changes in λ change the orbit parameters, are determined by the intersection points of the orbit.

Therefore, it is enough to identify the values of λ where the product $\lambda\bar{\rho}$ matches with the radial coordinates of all of the intersections of the nearby petals,

$$\lambda_k = \left[\frac{1-\epsilon}{1-\epsilon\cos(\pi k)}\right]^{\frac{1}{1-\eta}}. \tag{D3}$$

In the equation above, $k \in \mathbb{Z}$. Since the cosine function is not monotonic, the sequence of intersection distances from the origin does not automatically follow from the sequence of k. The bottom line is that the orbital parameters change with respect to λ discretely only at $\lambda = \lambda_k$ and otherwise remain unaltered. In other words, m, n, and χ are sectionally constant functions of the parameter λ.

[1] T. W. B. Kibble, J. Phys. A **9**, 1387 (1976).
[2] H. B. Nielsen and P. Olesen, Nucl. Phys. **61B**, 45 (1973).
[3] Pierre Auclair *et al.* (LISA Cosmology Working Group), J. Cosmol. Astropart. Phys. 04 (**2020**) 034.
[4] Y. Cui and D. E. Morrissey, Phys. Rev. D **79**, 083532 (2009).
[5] A. Albrecht and N. Turok, Phys. Rev. D **40**, 973 (1989).
[6] M. A. Fernandez, S. Bird, and Y. Cui, Phys. Rev. D **102**, 043509 (2020).
[7] D. G. Figueroa, M. Hindmarsh, and J. Urrestilla, Phys. Rev. Lett. **110**, 101302 (2013).
[8] L. M. Krauss, Phys. Lett. B **284**, 229 (1992).
[9] Y. Cui, M. Lewicki, and D. E. Morrissey, Phys. Rev. Lett. **125**, 211302 (2020).
[10] O. S. Sazhina, J. Exp. Theor. Phys. **116**, 71 (2013).
[11] O. S. Sazhina, D. Scognamiglio, and M. V. Sazhin, Eur. Phys. J. C **74**, 2972 (2014).
[12] B. P. Abbott *et al.* (LIGO Scientific and Virgo Collaborations), Phys. Rev. Lett. **116**, 061102 (2016).
[13] B. P. Abbott *et al.* (LIGO Scientific and Virgo Collaborations), Phys. Rev. Lett. **119**, 161101 (2017).
[14] B. P. Abbott *et al.* (LIGO Scientific and Virgo Collaborations), Astrophys. J. Lett. **896**, L44 (2020).
[15] S. Blasi and V. Brdar and K. Schmitz, Phys. Rev. Lett. **126**, 041305 (2021).
[16] J. Ellis and M. Lewicki, Phys. Rev. Lett. **126**, 041304 (2021).
[17] S. Chigusa, Y. Nakai, and J. Zheng, Phys. Rev. D **104**, 035031 (2021).
[18] W. A. Hiscock, Phys. Rev. D **31**, 3288 (1985).
[19] B. Linet, J. Math. Phys. (N.Y.) **27**, 1817 (1986).
[20] J. R. Gott, Astrophys. J. **288**, 422 (1985).
[21] M. F. A. da Silva, L. Herrera, F. M. Paiva, and N. O. Santos, J. Math. Phys. (N.Y.) **36**, 3625 (1995).
[22] L. Herrera, N. O. Santos, A. F. F. Teixeira, and A. Z. Wang, Classical Quantum Gravity **18**, 3847 (2001).
[23] L. Marder, Proc. R. Soc. A **244**, 524 (1958).
[24] A. Kleber, C. A. P. Galvao, and A. F. F. Teixeira, J. Phys. A **13**, 503 (1980).
[25] W. B. Bonnor, in *On Einstein's Path: Essays in Honor of Engelbert Schucking*, 1st ed., edited by A. Harvey (Springer Science+Business Media, New York, 1999), Chap. 8, pp. 113–119.
[26] Ł. Bratek, J. Jałocha, and M. Kutschera, Phys. Rev. D **105**, 023013 (2022).
[27] W. B. Bonnor and M. A. P. Martins, Classical Quantum Gravity **8**, 727 (1991).
[28] A. Z. Wang, M. F. A. da Silva, and N. O. Santos, Classical Quantum Gravity **14**, 2417 (1997).
[29] L. Herrera and N. O. Santos, J. Math. Phys. (N.Y.) **39**, 3817 (1998).
[30] I. Brito, M. F. A. da Silva, F. C. Mena, and N. O. Santos, Gen. Relativ. Gravit. **46**, 1681 (2014).
[31] M. N. Célérier, R. Chan, M. F. A. da Silva, and N. O. Santos, Gen. Relativ. Gravit. **51**, 149 (2019).
[32] B. Hoseini, R. Saffari, S. Soroushfar, S. Grunau, and J. Kunz, Phys. Rev. D **94**, 044021 (2016).
[33] J. F. Ritt, Trans. Am. Math. Soc. **27**, 68 (1925).
[34] H. Goldstein, C. P. Poole, and J. Safko, Hamilton-Jacobi theory and action-angle variable, in *Classical Mechanics*, 3rd ed. (Pearson Education, London, 2001), Chap. 10, pp. 430–482.
[35] A. S. Kompaneyets, Motion in a central field, in Theoretical Physics, 1st ed. (Foreign Language Publishing House, Moscow, 1961), Chap. 5, pp. 041–048.
[36] G. Birkhoff and G. Rota, First-order differential equations, in *Ordinary Differential Equations*, 4th ed. (John Wiley and Sons, New Jersey, 1991), Chap. 1, pp. 001–033.
[37] C. W. Misner and K. S. Thorne and J. A. Wheeler, The "pit in the potential" as the central new feature of motion in Schwarzschild geometry, in *Gravitation*, PUP ed. (Princeton University Press, New Jersey, 2017), Chap. 25, pp. 641–649.
[38] M. de León, P. D. Prieto-Martínez, N. Román-Roy, and S. Vilariño, J. Math. Phys. (N.Y.) **58**, 092901 (2017).
[39] K. Aomoto and M. Kita, Introduction: The Euler-Gauss hypergeometric function, in *Theory of Hypergeometric Functions* (Springer Science+Business Media, New York, 2011), 1st ed., Chap. 1, pp. 1–18.
[40] S. Weinberg, The principle of equivalence, in *Gravitation and Cosmology: Principles and Applications of the General Theory of Relativity*, 1st ed. (John Wiley and Sons, New York, 1972), Chap. 3, pp. 70–79.
[41] J. L. Synge, Fields with spherical symmetry, in *Relativity: The General Theory*, 1st ed. (North-Holland Publishing Company, Amsterdam, 1960), Chap. 8, pp. 289–298.
[42] H. Goldstein, C. P. Poole, and J. Safko, Classical chaos, in *Classical Mechanics*, 3rd ed. (Pearson Education, London, 2001), Chap. 11, p. 483.
[43] J. Levin and G. Perez-Giz, Phys. Rev. D **77**, 103005 (2008).
[44] J. V. José and E. J. Saletan, Topics in Hamiltonian dynamics, in *Classical Dynamics: A Contemporary Approach*, 1st ed. (Cambridge University Press, Cambridge, England, 1998), Chap. 6, pp. 284–307.

[45] C. W. Misner, K. S. Thorne, and J. A. Wheeler, Riemannian geometry: Metric as foundation of all, in *Gravitation*, PUP ed. (Princeton University Press, New Jersey, 2017), Chap. 13, pp. 315–323.
[46] M. Henneaux and C. Teitelboim, Constrained Hamiltonian systems, in *Quantization of Gauge Systems*, 1st ed. (Princeton University Press, New Jersey, 1992), Chap. 1, pp. 003–041.
[47] U. H. Gerlach, Phys. Rev. **177**, 1929 (1969).
[48] E. Hackmann and C. Lämmerzahl, Phys. Rev. Lett. **100**, 171101 (2008).